THE DEVELOPMENT OF FT-RAMAN TECHNIQUES TO QUANTIFY THE HYDROLYSIS OF COBALT(III) NITROPHENYLPHOSPHATE COMPLEXES USING MULTIVARIATE DATA ANALYSIS

by

OUPA SAMUEL TSHABALALA

Submitted in fulfilment of the requirements for
the degree

MASTER OF SCIENCE

in the subject

CHEMISTRY

at the

UNIVERSITY OF SOUTH AFRICA

SUPERVISOR: PROFESSOR S. O. PAUL (PhD)

JOINT SUPERVISOR: PROFESSOR F. TAFESSE (PhD)

MARCH 2007

DECLARATION

Student number: 35315377

I declare that THE DEVELOPMENT OF FT-RAMAN TECHNIQUES TO QUANTIFY THE HYDROLYSIS OF COBALT(III) NITROPHENYL-PHOSPHATE COMPLEXES USING MULTIVARIATE DATA ANALYSIS is my own work and that all the sources that I have used or quoted have been indicated and acknowledged by means of complete references.

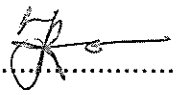

SIGNATURE

(Mr O.S. Tshabalala)

12/06/07

DATE

ACKNOWLEDGEMENTS

It is not possible for me to mention all people who contributed or added value to my academic, social and spiritual life towards the completion of this dissertation. As a matter of fact this work would not be fruitful, educational and memorable without wisdom and intelligence of some coaching and positive criticism. In nutshell, I would like to express my sincere and fraternal gratitude to the following people:

Above all: I thank my Father God, and my Lord Jesus Christ, and my comforter the Holy Spirit for revealing the purpose of my existence and life. JESUS IS LORD!

Professor S. O. Paul (PhD), my Supervisor: for her expertise in Vibrational Spectroscopy and its related theory, and Chemometrics; for her availability and guidance in my research work.

Professor F. Tafesse (PhD), my Joint-Supervisor: for his expertise in the field of Inorganic Chemistry, and metal-organophosphates complexes; for his advices and guidance in my research work.

Mr D. C. Lilies (Dave), crystallography specialist form the Department of Chemistry (University of Pretoria, RSA), for his availability to determine the structure of $[Co(tn)_2CO_3]ClO_4$ using crystallographic method.

The University of South Africa (UNISA), in particular, the Department of Chemistry for their financial contribution in my MSc studies. Moreover, Chemistry department staff, Colleagues and Friends for all their direct and/or indirect support.

The Tshabalala family: I give gratitude to my wife Mokgadi and my daughter Bontle, my parents Wilson and Magdalene, my brother Abram and my sister Linda, for their encouragement and support in my studies.

ABSTRACT

The FT-Raman techniques were developed to quantify reactions that follow on mixing aqueous solutions of bis-(1,3-diaminopropane)-diaquacobalt(III) ion ($[Co(tn)_2(OH)(H_2O)]^{2+}$) and *p*-nitrophenyl-phosphate (PNPP).

For the development and validation of the kinetic modelling technique, the well-studied inversion of sucrose was utilized. Rate constants and concentrations could be estimated using calibration solutions and modelling methods. It was found that the results obtained are comparable to literature values. Hence this technique could be further used for the $[Co(tn)_2(OH)(H_2O)]^{2+}$ assisted hydrolysis of PNPP.

It was found that rate constants where the pH is maintained at 7.30 give results which differ from those where the pH is started at 7.30 and allowed to change during the reaction. The average rate constant for 2:1 ($[Co(tn)_2(OH)(H_2O)]^{2+}$:PNPP reactions was found to be approximately 3×10^4 times the unassisted PNPP hydrolysis rate.

Keywords: FT-Raman, kinetic modelling, partial least squares, multivariate data analysis, sucrose hydrolysis, *p*-nitrophenylphosphate, *p*-nitrophenol, cobalt(III) complex, organophosphate ester hydrolysis, pseudo-first order rate constant and second order rate constant.

TABLE OF CONTENTS

LIST OF TABLES

LIST OF FIGURES

LIST OF ACRONYMS

KM	Kinetic Modelling
MDA	Multivariate Data Analysis
PC	Principal Component
PLS	Partial least squares
PNPP	*p*-Nitrophenylphosphate
PNP	*p*-Nitrophenol
PRESS	Prediction Residual Error Sum of Squares
RMSD	Root mean squared deviation
tn	1,3-Diaminopropane

CHAPTER 1

Introduction

1.1 Research motivation

The research work presented in this dissertation is part of the ongoing investigation[1] on metal ion assisted hydrolysis of organophosphates (or phosphate esters). The understanding of organophosphate hydrolysis is very important in biological and environmental sciences[2-7,8,9]. The general organophosphate hydrolysis is shown in Figure 1.1, where substituents R_1 and R_2 can either be the alkyl or aryl group, whereas substituent OX is the leaving group during the substitution reaction (the hydrolysis).

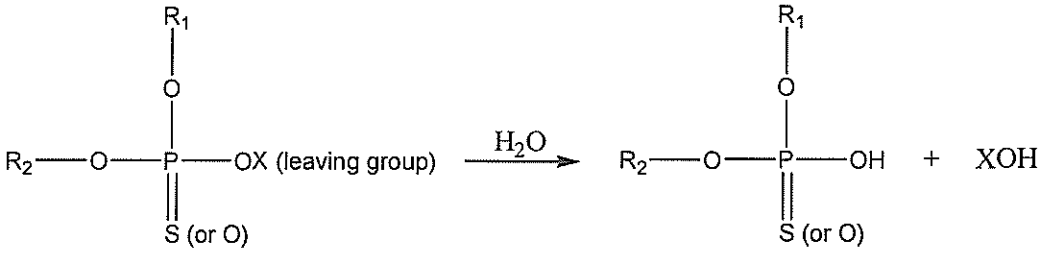

Figure 1.1 General organophosphate hydrolysis

In general organophosphates are very slow to undergo hydrolysis[8]; hence metal complexes are used to enhance these reactions. Although organophosphate compounds and their metal assisted hydrolysis are mostly studied using methods such as HPLC[10], IR spectroscopy[11,12], NMR[13-15] spectroscopy and UV/VIS[1,16-25] spectrometry, Raman

spectroscopy has not been used to monitor the hydrolysis of these compounds.

In this present research work much emphasis is put on developing FT-Raman techniques to compliment existing methods for the estimations of rate constants in the hydrolysis of organophosphates. The reaction of interest in this work, the bis-(1,3-diaminopropane)aquahydroxo-cobalt(III) ion ($[Co(tn)_2(OH)(H_2O)]^{2+}$) assisted hydrolysis of *p*-nitrophenylphosphate (PNPP) has been previously examined using NMR spectroscopy and UV/VIS spectrometry[13], where it was used as a model for the decontamination of organophosphates in the environment[1,9].

Although $[Co(tn)_2(OH)(H_2O)]^{2+}$ precursors are not commercially available, procedures to synthesize the required amount for the PNPP hydrolysis are known[9,26,27]. One reason to use $[Co(tn)_2(OH)(H_2O)]^{2+}$ in the hydrolysis of PNPP is that the Co–N bond has been reported to be stable for a long time and it is not photo-decomposed by NIR lasers[9].

1.2 Statement of problem

In this work, $[Co(tn)_2(OH)(H_2O)]^{2+}$ is used to enhance the hydrolysis of PNPP, but it does not act as a catalyst because it forms a stable phosphate-$Co(tn)_2$ complex[13]. The problem encountered with these kinds of reactions is that PNPP and $[Co(tn)_2(OH)(H_2O)]^{2+}$ solutions cannot be calibrated because they react. This implies that rate constants for the $[Co(tn)_2(OH)(H_2O)]^{2+}$ assisted hydrolysis of PNPP cannot be estimated using calibration methods. For this purpose, FT-Raman techniques and multivariate data analysis (MDA) could be developed as an alternative method to quantify the hydrolysis of PNPP.

1.3 Literature review on applications of Raman spectroscopy and multivariate data analysis (MDA) in organophosphates

The historical and theoretical aspects of FT-Raman spectroscopy and MDA (which is part of chemometrics) will be discussed in the next chapter (Chapter 2); it will also include reasons for using these techniques. A limited number of applications of Raman spectroscopy and chemometrics on reactions of organophosphates is recorded in the literature[10,28-33].

Tanner et al.[32] applied FT-Raman spectroscopy to collect spectra of pesticides. About fourteen different pesticides were qualitatively analysed and their Raman peaks were assigned. They characterised and described various spectral modes such as P=O stretch at 1304 to 1209 cm^{-1}. Skoulika et al.[29,30] were the first group to quantify pesticide formulations using FT-Raman spectroscopy. Raman spectra of fenthion[29] in pesticides were quantitatively analysed. Concentrations of fenthion were determined using calibration curves based on peak area.

In their subsequent work[30], Skoulika et al. used chemometrics (both univariate and multivariate calibration) to quantify methylparanthion found in pesticide formulations. Univariate calibration methods use one variable such as spectral peak or area to develop a regression model whereas multivariate calibration methods use several variables to develop a regression model. Their multivariate calibration was based on stepwise multiple linear regression (MLR) to determine concentrations of samples. In their work, both methods give similar results. Another

group, Farquharson et al.[34] studied the Raman spectra of VX (a nerve gas) and its hydrolysis products using Surface-enhanced Raman Spectroscopy. In their analysis of VX and hydrolysis products, Raman peaks at 1015-1103, 971-945, 905-885 and 744-721 cm^{-1} are assigned to PO_n bend, PO_n stretch, OPC or CCN stretches and PC stretch, respectively.

1.4 Research objectives

The purpose of this investigation is as follows:

1 The main objective of this research project is to attempt to develop the complimentary techniques to estimate rate constants of $[Co(tn)_2(OH)(H_2O)]^{2+}$ assisted hydrolysis of PNPP.

2 The preliminary objective is to develop and to validate FT-Raman techniques and the partial least squares (PLS) version of MDA using the hydrochloric acid catalysed inversion of sucrose. The hydrochloric acid catalysed inversion of sucrose was chosen because it is user friendly, its reagents are readily available and commercially affordable, and the order and rate constants, including its hydrolysis products, are well-known[35,36].

CHAPTER 2

Historical and theoretical aspects of FT-Raman spectroscopy and multivariate data analysis

2.1 FT-Raman techniques and multivariate data analysis

The Fourier transform (FT)-Raman techniques in this work refer to the combination of several methods viz. the online sampling system, FT-Raman spectrometer and kinetic modelling method. The online sampling system is a loop system connected to the single flow-through cell and the sample vessel. This loop uses a peristaltic pump to circulate the sample. In addition to FT-Raman techniques, the partial least squares (PLS) version of multivariate data analysis (MDA) is used to quantify the FT-Raman spectra of reactions. Some information about the history and theory of FT-Raman spectroscopy and PLS-MDA are discussed.

2.2 FT-Raman spectroscopy

2.2.1 History of Raman spectroscopy development

Light scattering by molecules which are illuminated is known as the Raman effect[37-44]. The theory of light scattering by molecules was predicted in 1923 by Smekal. Five years later, in 1928, Sir C. Raman was the first person who observed the scattering of light and for that discovery he was awarded the Nobel Prize. By 1939 conventional Raman, using diffraction gratings and mercury lamps for illumination, was in use.

Major developments of Raman spectroscopy can be traced back to the 1960s when lasers were developed and could be used as the illumination source. Hendra et al.[39] cites Chase and Hirschfeld to have suggested the possibility of using near-infrared (NIR) lasers and interferometers. As from 1986, applications of FT-Raman have increased remarkably and it has recently found applications in the analysis of organophosphates[29,30,39]. FT-Raman spectroscopy in this work is used as the method for kinetic studies.

2.2.2 Basic concepts

When a sample is illuminated with monochromatic radiation[37-41], some photons are scattered by the sample as shown in Figure 2.1. Most of the scattered photons possess the same wavelength as the incident photons. This phenomenon is referred to as the elastic or Rayleigh scattering. Few photons (approximately 1 in 10,000,000) are scattered at a wavelength different to that of the incident photons. This wavelength shift is called

inelastic scattering or Raman scattering. Most of these scattered photons are shifted to wavelengths which are longer than the incident radiation (Stokes shift), while the rest are shifted to shorter wavelengths (anti-Stokes shift). Stokes-shifted peaks are more intense than anti-Stokes shifted peaks and are therefore preferably used.

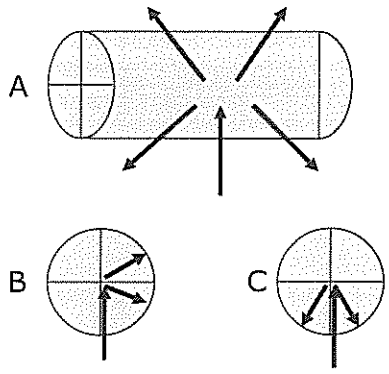

Figure 2.1 Light scattering in cylindrical liquid sample arrangements: A. the cylindrical tube showing some scattering, B. components of perpendicular scattering (90°) and C. components of back scattering (180°).

The wavelength shift is a measure of vibrations for a specific molecule. A linear molecule with n atoms possesses 3n-5 and a non-linear molecule possesses 3n-6 normal frequency modes of vibration, where n is the number of atoms in the molecule. Atoms in a molecule can be modelled by masses connected to each other by springs (from Hooke's law). A diatomic molecule model is commonly used to illustrate the relationship between atoms and vibrations because it has one normal frequency mode of vibration.

The vibrational frequency (v_{vib}) and the reduced mass (μ) of a diatomic molecule are related as follows:

$$v_{vib} = \frac{1}{2\pi}\sqrt{\frac{k}{\mu}} = \frac{1}{2\pi}\sqrt{\frac{k(m_1+m_2)}{m_1 m_2}} \qquad (2.1)$$

where

k is a force constant,

m_1 is the mass of atom 1, and

m_2 is the mass of atom 2.

Monochromatic radiation that is incident to a sample has an electric and a magnetic field that simultaneously oscillate perpendicular to each other and to the direction of propagation. The electric field on that radiation causes a movement of a cloud of electrons around nuclei. This kind of temporary distortion happens by creating a polarity of electrons relative to its nuclei, thus the induction of dipole moment (μ_{ind}). In terms of the electric field, the Stokes scattering can now be represented by,

$$\mu_{ind} \propto \left(\frac{\partial \alpha}{\partial Q_{vib}}\right)_o \frac{E_o Q_o}{2} \cos 2\pi(v_o - v_{vib}) \qquad (2.2)$$

where

Q_{vib} is the normal coordinate,

α is the proportionality constant (or the polarizability of a molecule),

Q_o is the vibrational amplitude, and

E_o is the amplitude of the electric field.

v_o is the frequency of the incident beam (or radiation)

v_{vib} is the frequency of vibration of the molecule.

To observe Raman scattering, the polarizability of a molecule (sample) must be changing with respect to the normal coordinates (that is, $\partial\alpha/\partial Q_{vib} \neq 0$) when it is illuminated with monochromatic radiation.

As discussed earlier, some of the incident and the scattered photons possess different wavelengths. This change in wavelength (Raman scattering) is due to the interaction between photons and atoms in a molecule. Stokes scattering is illustrated in Figure 2.2 below. The virtual energy in the figure is an energy level between the ground and the first excited electronic state. The energy change (ΔE) is observable as the band characterising a molecule's mode of vibration.

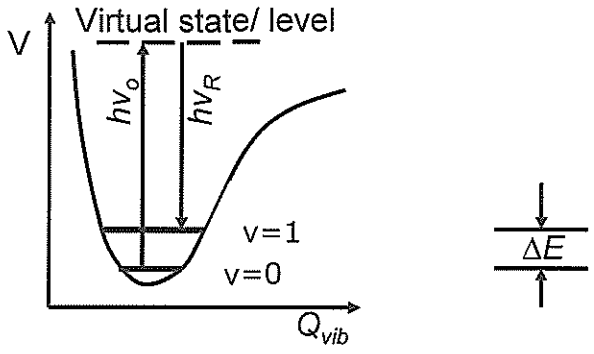

Figure 2.2 Stokes Raman scattering. Q_{vib} is a normal coordinate, V is the potential energy, v is the vibrational energy state, ΔE ($h\nu_{vib}$) is the change in energy due to scattering, $h\nu_o$ is the incident photon's energy and $h\nu_R$ is the scattered photon's energy.

The mathematical representation of the figure above is given by the following:

$$h\nu_{vib} = h\nu_{o} - h\nu_{R(St)} \qquad (2.3)$$

Where

h is the Planck's constant

$\nu_{R(St)}$ is the frequency of Raman Stokes scattering

ν_{o} is the frequency of the incident radiation

2.2.3 Advantages of FT-Raman spectroscopy

Raman spectroscopy can be used as alternative or complementary method for the vibrational characterization of molecules. Although the Raman scattering measured is several magnitudes less intense than the signals recorded for absorption of infrared radiation by molecules, there are several advantages. Some of the advantages[45-48] of Raman and/or FT-Raman spectroscopy are as follows:

***Sample Analysis*:** It is possible to use glass or quartz cells or tubes to hold samples in Raman spectroscopy. Unlike UV-vis, NMR, HPLC and other analytical methods, no sample preparation such as mulling agent for solids is required.

***Sampling*:** It is possible to collect FT-Raman spectra for real time monitoring[49] of reactions. The monitoring can be done in-situ or online.

***Laser source*:** The use of a NIR laser such as 1064nm Nd:YAG reduces if not virtually eliminates fluorescence and photochemical effects.

***Recording*:** It is possible to record Raman spectra with high resolution[40,48] (≥ 1) for accurate determination. A Nd:YAG laser is fairly stable (with long term stability of ±3%)[47] and it can be used to irradiate the sample for a sequence of scans.

***Spectrum*:** The Raman spectrum for water is weak and not obstructive as compared to strong broad bands of IR spectra observed for aqueous solutions.

2.3 Partial least squares version of multivariate data analysis

2.3.1 Historical background

The application of the chemometrics version of PLS has been known for about 27 years since its introduction in the late seventies. In the interview recorded by Geladi and Esbensen[50] (chemometricians), Kowalski mentions using multivariate methods from the 1960s. Kowalski, Wold and Massart are noted as respected originators of chemometrics. Despite its uncertain beginnings in 1972, chemometrics was fully recognised in 1974 as a field of study. In addition to the originators in the 1970s, Christie, Clementi, Hopke, Martens, Brown and Deming[51] were very active chemometricians. MDA has recently been applied to spectral data of organophosphates[29,30].

2.3.2 Basic principles

MDA is a chemometrics method which involves the analysis of many variables at the same time. These variables are sets of observable (or independent) and dependent data which can be correlated. Since FT-Raman spectra of some reactions cannot be quantified using univariate methods, so PLS regression can be used for analysing correlations between variables. More information on PLS multivariate data analysis can be found in the literature[50-68].

For analytical purposes, if several spectra of n samples of known concentrations are collected, their spectral data and concentrations could be used to form a MDA training set. The spectral data can be represented as a matrix **X** of nxp dimensions, for a single Raman spectrum, n is equals to one and each column of p is the intensity at a given wavenumber. On the other hand, the concentration data can be represented by an nxm **Y** matrix, where m is the number of components in the sample.

Pre-processing of data, for instance mean centering, is very important in PLS regression development as illustrated in Figure 2.3 below. Mean centering organises the scattered original data by adjusting it to the average value.

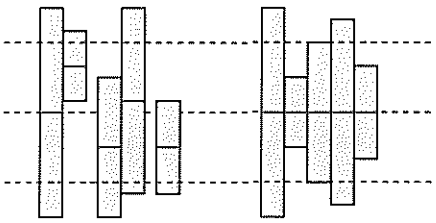

Figure 2.3 Illustration of pre-processing: (A) original or raw data and (B) mean centered data.

The mathematical description of mean centering in Figure 2.3 is as follows: the mean centering of data is calculated by subtracting the mean from the original data as shown by equations 2.4 and 2.5.

$$\bar{x}_k = \frac{\sum_{i=1}^{n} x_{ik}}{n} \tag{2.4}$$

$$x_{ik}^{centered} = x_{ik} - \bar{x}_k \tag{2.5}$$

where

k is the x-variable index,

i is the sample index, and

n is the number of samples.

2.3.3 PLS regression model

PLS is the method that uses concentration information (**Y**) while it decomposes spectral matrices (**X**). The spectral and constituent concentration data are transformed into eigenvectors and scores at the same time. The scores formed are orthogonal (that is, independent) and they are predictors of **Y** as they model **X**.

$$t_{ia} = \sum_k w^*_{ka} x_{ik} \; ; \qquad (\mathbf{T} = \mathbf{X}\mathbf{W}^*) \tag{2.6}$$

where

t_{ia} (scores, **T**) are linear combinations of **X** with weights,

w_{ka} (weights, **W**) are coefficients of **X**,

x_{ik} (**X**) are the original variables, and

a = 1,2,...,A is the index of components

In the PLS model X-scores are multiplied by loadings (p_{ak}, **P**) such that residuals (e_{ik}, **E**) are minimised.

$$x_{ik} = \sum_a t_{ia} p_{ak} + e_{ik} \qquad (\mathbf{X} = \mathbf{T}\mathbf{P}' + \mathbf{E}) \tag{2.7}$$

Similarly, Y-scores are multiplied by weights to make residuals very small,

$$y_{im} = \sum_a u_{ia} c_{am} + g_{im} \qquad (\mathbf{Y} = \mathbf{U}\mathbf{C}' + \mathbf{G}) \tag{2.8}$$

where

y_{im} (**Y**) are predictable variables,

u_{ia} (**U**) are scores,

c_{am} (**C**) are weights,

g_{im} (**G**) are residuals, and

m is the y-variable index

Since the idea of PLS regression is to predict **Y** variables using X-scores, equation 2.8 can be written in terms of

$$y_{im} = \sum_a c_{am} t_{ia} + f_{im} \qquad (\mathbf{Y} = \mathbf{TC}' + \mathbf{F}) \tag{2.9}$$

When combining both equations 2.6 and 2.8, PLS regression coefficients (which are not orthogonal) can be deduced as

$$b_{mk} = \sum_a c_{ma} w^*_{ka} \; ; \qquad (\mathbf{B} = \mathbf{W}^*\mathbf{C}') \tag{2.10}$$

which can then be used for the prediction of unknown concentrations.

2.3.4 Number of components, correlation of variables and prediction error

The performance of a PLS, a multivariate regression model, is based on finding the correct or optimum number of components (that is, model dimensionality). These components are determined by comparing the predicted variables (**Yp**) to the known (or reference) variables (**Yk**). The correctness of the model is found when the difference between **Yk** and **Yp** is at the minimum as number of components are added. That is, the optimum number of components is found at the minimum prediction residual error sum of squares (PRESS).

$$PRESS = \sum_{i=1}^{n} (Yk_i - Yp_i)^2 \tag{2.11}$$

Correlation of variables is sometimes referred to as the correlation coefficient (R) or coefficient of multiple determinations (R^2). The coefficient of multiple determinations is such that $0 \leq R^2 \leq 1$ (Equation 2.12) and is the measure of the interdependence between **Yk** and **Yp** variables and it will be used later.

$$R^2 = \frac{\sum_{i=1}^{n} \left(Yp_i - \overline{Yk}\right)^2}{\sum_{i=1}^{n} \left(Yk_i - \overline{Yk}\right)^2} = \frac{\sum_{i=1}^{n} \left[\left(Yk_i - \overline{Yk}\right)\left(Yp_i - \overline{Yp}\right)\right]^2}{\left(\sum_{i=1}^{n} \left(Yk_i - \overline{Yk}\right)^2\right)\left(\sum_{i=1}^{n} \left(Yp_i - \overline{Yp}\right)^2\right)} \tag{2.12}$$

In this work, a difference between values predicted by the model (theory) and values from experimental data will be measured. The reliability (or error) of a model to estimate can be measured by bias (prediction bias) and/or root mean squared deviation (RMSD). The less the bias or RMSD values become, the more the model becomes reliable, vice-versa.

$$Bias = \frac{\sum_{i=1}^{n} (Yk_i - Yp_i)}{n} \tag{2.13}$$

$$RMSD = \sqrt{\frac{\sum_{i=1}^{n} (Yk_i - Yp_i)^2}{n}} \tag{2.14}$$

2.3.5 Advantages of using PLS technique

1 PLS is more advantageous than Multiple Linear Regression (MLR) methods such as classical least squares (CLS) and inverse least squares (ILS)[66]. In fact, PLS was developed with the full spectral coverage of CLS and with partial composition regression of ILS.

2 PLS is a full-spectrum method that is related and also superior to other full-spectrum methods such as principal component regression (PCR). The superiority and advantage of PLS can be recognised in its ability to average signals, to detect outliers and to obtain limited interpretable spectral information.

In this research work, the ability of FT-Raman techniques, in combination with the PLS version of multivariate data analysis, to quantify reactions will be demonstrated. Firstly, the development of these techniques using the acid catalysed inversion of sucrose will be discussed in Chapter 3. Secondly, the applications of the developed techniques, together with the PLS, for the estimation of rate constants of bis-(1,3-diaminopropane)aquahydroxycobalt(III) perchlorate assisted hydrolysis of *p*-nitrophenylphosphate will be discussed in Chapter 4.

CHAPTER 3

The development of FT-Raman techniques using the acid catalysed inversion of sucrose

3.1.1 Introduction

The hydrochloric acid catalysed inversion of sucrose is a well known hydrolysis reaction because it has been frequently used for kinetics studies[35,36,69-83] of reactions in general, and it has been reported to be a pseudo-first order reaction. In the previous investigation of this reaction, pseudo-first order rate constants were estimated using polarimetry[35] and infrared spectroscopy[36]. It was also shown that the inversion of sucrose is dependent on the hydrochloric acid.

Although previous Raman and IR studies of sucrose, fructose and glucose have been recorded in the literature[36,84-99], the goal of this part of the research work was to re-estimate rate constants of the inversion of sucrose at various concentrations of hydrochloric acid for the sake of developing the Fourier transform (FT)-Raman techniques, which is a combination of an online sampling system, an FT-Raman spectrometer and kinetic modelling. In addition, the PLS version of MDA has been applied. It will be shown that kinetic modelling can successfully replace the commonly used calibration method for the estimation of rate constants.

3.1.2 Determination of pseudo-first and second order rate constants

The hydrochloric acid (HCl) catalysed inversion of sucrose to form fructose and glucose,

$$\underset{\text{sucrose}}{C_{12}H_{22}O_{11}} + H_2O \xrightarrow{HCl} \underset{\text{fructose}}{C_6H_{12}O_6} + \underset{\text{glucose}}{C_6H_{12}O_6} \qquad (3.1)$$

is a pseudo first order reaction[35,36] if the consumption of sucrose (S) follows the rate:

$$v = \frac{d[S]}{dt} = -k_1[S] \qquad (3.2)$$

where H_2O is in excess because it is used as a solvent. As a result, it is not part of equation 3.2. Since the pseudo first order rate constant (k_1) has been reported to be dependant on the concentration of the hydrogen ion of HCl, it can be expressed by the following relation:

$$k_1 = k_2[H^+] \qquad (3.3)$$

where k_2 is a second order rate constant. The integrated law for equation 3.2 (from initial conditions: t = 0 and $[S]_0$) is given by,

$$[S] = [S]_o e^{-k_1 t} \qquad (3.4)$$

Equation 3.4 will be used to estimate pseudo first order rate constants for the acid catalysed inversion of sucrose. To theoretically calculate several concentrations of sucrose using selected rate constants for each

reaction at the same time, equation 3.4 shown above can be presented in a matrix form of ixj dimensions

$$[S]_{ij} = [S]_o e^{-k_{1j}t_i} \qquad (3.5)$$

where i = 1, 2, 3,... is the number of samples and j = 1, 2, 3,... is the number of the selected range of pseudo first order rate constants. This equation will be used in the subsequent kinetic modelling.

3.1.3 Kinetic Modelling

The common procedure for the estimation of rate constants begins by developing a calibration method. Then the predicted concentrations of the analyte using the pre-developed calibration method are plotted with respect to reaction time. Ultimately, rate constants are estimated by fitting a curve, exponential function in this case, through the plotted data points. The constant value in the exponential function is the pseudo-first order rate constant required for the reaction. In this work more emphasis is put on estimating the rate constant using kinetic modelling instead of the calibration method. The procedure for the FT-Raman modelling technique is executed as follows:

Step 1 Starts by arranging FT-Raman spectra and guessing a range of rate constants of a specific order of reaction for the kinetic modelling. A prior knowledge of the rate constant for each reaction is advantageous because a range of rate constant can be estimated quickly. A better way to select a rate constant is to start with a wide range and then narrow it in an iterative manner.

Step 2 Use equation 3.5, selected pseudo-first order rate constants and the recorded reaction time for each spectrum to model concentrations of sucrose consumption, creating an ixj matrix form of sucrose concentration. For example, see Table 3.1 below.

Table 3.1 An example of an ixj matrix created for sixty samples. t_1(min) refers to time in minutes and k_{1j}(min^{-1}) refers to pseudo-first order rate constant.

		j	1	2	3	4	5	6	7	8	9
		k_{1j} (min^{-1})	0.0180	0.0190	0.0200	0.0210	0.0220	0.0230	0.0240	0.0250	0.0260
i	t_i (min)										
1	3		0.9474	0.9474	0.9474	0.9474	0.9474	0.9474	0.9474	0.9474	0.9474
2	6		0.8976	0.8976	0.8976	0.8976	0.8976	0.8976	0.8976	0.8976	0.8976
3	9		0.8504	0.8504	0.8504	0.8504	0.8504	0.8504	0.8504	0.8504	0.8504
4	12		0.8057	0.8057	0.8057	0.8057	0.8057	0.8057	0.8057	0.8057	0.8057
5	15		0.7634	0.7634	0.7634	0.7634	0.7634	0.7634	0.7634	0.7634	0.7634
6	18		0.7233	0.7233	0.7233	0.7233	0.7233	0.7233	0.7233	0.7233	0.7233
.	.		.								.
.	.		.								.
.	.		.								.
60	180		0.0392	0.0392	0.0392	0.0392	0.0392	0.0392	0.0392	0.0392	0.0392

Step 3 The calculated concentrations of sucrose in step 2, together with FT-Raman spectra for each reaction, are used in this case to create a PLS-MDA training set, to determine the optimum principal component (PC) and to apply it in the PLS model. In PLS-MDA, a training set can be used for regression and validation purposes, in particular cross validation.

Step 4 The main purpose of this step is to estimate the optimised pseudo-first order rate constant ($k_{1,opt.}$). The

optimum value of the rate constant is determined by finding the maximum coefficient of multiple determinations (R^2_{max}) in a plot of R^2 versus k_1 (see the example shown in Figure 3.1 below). The coefficient of multiple determinations mentioned above is obtained from the PLS regression line (from step 3) of actual versus predicted concentrations of sucrose.

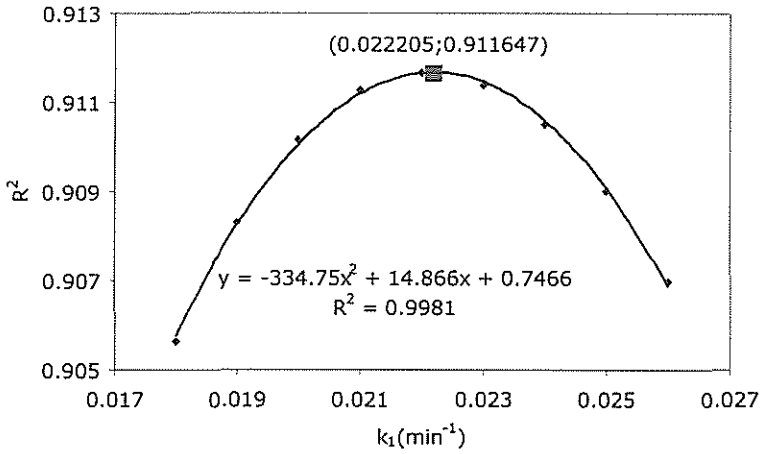

Figure 3.1 A plot of R^2 versus k_1. The value of 0.0222 min^{-1} for $k_{1,opt}$ is found at R^2_{max} of 0.9117.

Step 5 If the estimated $k_{1,opt.}$ is found in step 4, it can be used to further estimate concentrations of sucrose at any given time in a reaction using equation 3.4 above, or the second order rate constant using equation 3.3 above. On the contrary, if $k_{1,opt.}$ cannot be found, another range of pseudo-first order rate constants can be selected.

Therefore the discussed procedure can then be summarised by Figure 3.2 below (the procedure starts at the asterisk*).

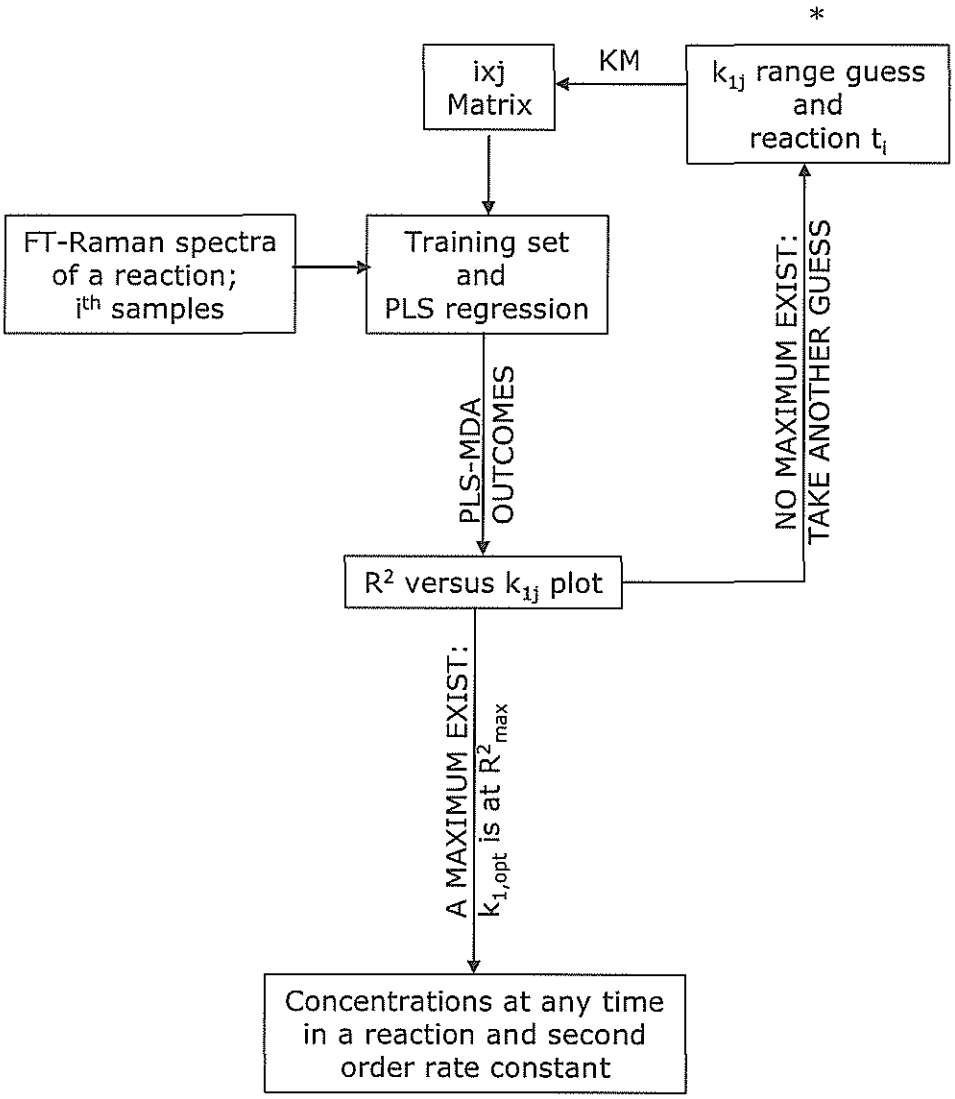

Figure 3.2 A chart for the estimations of rate constants using FT-Raman modelling technique.

3.2 Experimental

3.2.1 Reagents

All compounds of sucrose, fructose, glucose and hydrochloric acid used in this work were either analytical reagent or purest grade commercially available from Rochelle Chemicals and/or Saarchem (Merck), and were used without any further purification. Milli-Q water (conductance = 18 MΩ.cm) was used for all rinsing and preparations of solutions.

3.2.2 Instrumentation and software

Figure 3.3 is a typical experimental setup that was used for reactions; this is the online FT-Raman spectroscopy for the recording of spectra. As shown in the figure, sample solutions can be easily circulated from the sample vessel resting upon the magnetic stirrer plate (A) to the FT-Raman sampling compartment for the laser illumination (C) through silicon tubes attached to the Gilson minipuls 2 peristaltic pump (B) from Laboratory and Scientific (Lasec) equipment. This is the real time measuring process. The magnetic stirrer is used to stir the sample while it circulates through the tube. An MNR glass tube is used as a window for laser illumination and scattering.

The Raman spectrometer (Bruker FRS100 shown in Figure 3.3) is a computer operated instrument equipped with a 1064 nm Nd-YAG (NIR laser), a Michelson interferometer and a liquid nitrogen cooled Germanium detector. The laser illuminating power was set at 500 mW (contributing ~60% of radiation at the sample; estimated to be approximately 300 mW at the sample). Each spectrum of range 50 or 100 to 4000 cm^{-1} wavenumbers was recorded for reactions (where 128

scans were averaged). The resolution was set at 8 cm^{-1} wavenumbers for all spectral recordings.

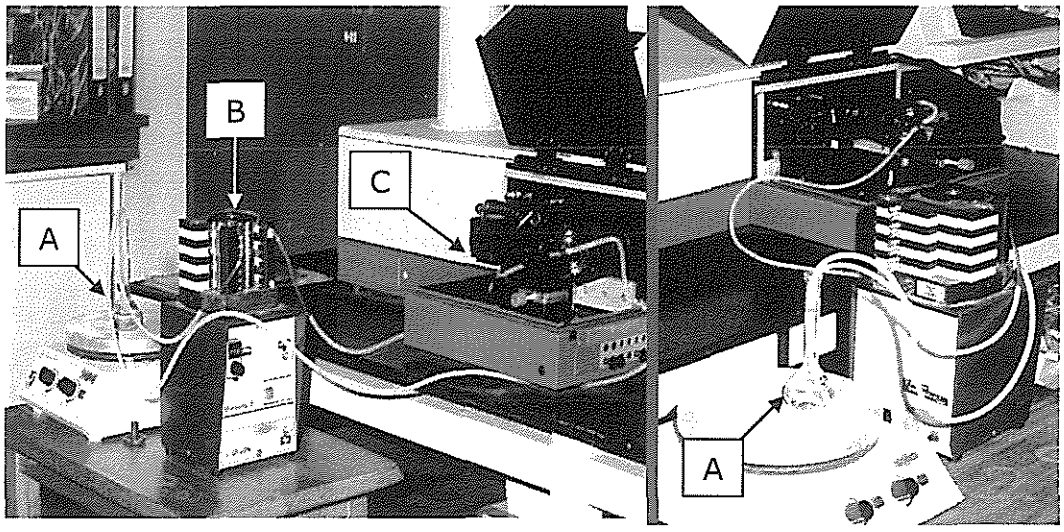

Figure 3.3 The online FT-Raman spectrometer: (A) reaction vessel, (B) peristaltic pump and (C) sample compartment. For kinetic measurements of a reaction, the solution is circulated from A to C through B. For safety assurance, the sample compartment of the Raman spectrometer used is always closed to avoid radiation exposure from the laser.

Raman parameters (number of scans and resolution) were chosen in order to accommodate a reasonable number of averaged scans for a good signal-to-noise ratio of the spectra during the hydrolysis reaction: they were chosen such that reactions could be monitored successfully when a spectrum was obtained at roughly 3 minute intervals. These parameters were operated and controlled by the computer installed with OPUS software (version 3.1 from Bruker Optik GmbH 1997-2000). For analysis purposes, PLS-MDA was performed with GRAMS 32[66] (or Unscrambler[52]) software packages.

3.2.3 Experimental procedure

The inversion reactions were initiated when 20 mL of 20 % (w/v) sucrose[82] solutions came into contact with 20 mL of several solutions of HCl (1.0106, 2.0212, 3.0318, 4.0424, 5.0530 and 6.1200 M) at room temperature (294.65-295.15 K) for three hours in order to record many spectra; for each reaction the total volume of solution was 40 mL. Initially sampling containers such as cuvettes and volumetric flasks were tried to sample reaction solutions, but they were found time consuming and labour intensive, in particular for the monitoring process. As a result, the online sampling system was used throughout the kinetic measurements.

For reference purposes, 20 % (w/v) solutions of sucrose, fructose and glucose were also scanned in the spectrometer for the analysis of spectral peaks which changed during the inversion reactions. To determine concentrations of sucrose, fructose and glucose for each reaction solution using the calibration method, calibration solutions[41] were prepared according to equation 3.6 and Table 3.2. HCl was not included when preparing calibration solutions because it catalyses the reaction, causing sucrose to decompose. To check the effect of HCl on the calibration solutions, FT-Raman spectra of two solutions (acidified with 5 M HCl and non-acidified) containing a mixture of 2.63 g fructose and 2.63 g glucose were also recorded.

$$\text{Mole ratio of F or G} = \frac{180.16^{a}}{342.30^{b}} \times (1 - X) = 0.5260 \times (1 - X) \qquad (3.6)$$

Where

[a] is the molar mass of fructose (F) or glucose (G),

^{b} is the molar mass of sucrose (G), and

X is the mole ratio of sucrose (as shown in Table 3.2)

Table 3.2 Mole ratios of sucrose, fructose and glucose in calibration mixtures

Sucrose	1.0000	0.8750	0.7500	0.6250	0.5000	0.3750	0.2500	0.1250	0.0000
Fructose	0.0000	0.0656	0.1315	0.1973	0.2630	0.3288	0.3945	0.4603	0.5260
Glucose	0.0000	0.0656	0.1315	0.1973	0.2630	0.3288	0.3945	0.4603	0.5260

3.3 Results and discussion

3.3.1 Analysis of Raman spectra and peaks

Since the inversion of sucrose involves the addition of hydrochloric acid as a catalyst[35,36,69-83] (refer to equation 3.1), and counting on the fact that hydrochloric acid was not included in the calibration solutions (refer to section 3.2.3), it was important to check the Raman spectra for the influence of hydrochloric acid on the products of the inversion reaction as shown in Figure 3.4.

In this figure, spectrum with solid line represents the Raman scattering of the solution made of 2.63 g fructose, 2.63 g glucose and 5 M HCl, and spectrum with broken line represents the Raman scattering of the solution made of 2.63 g fructose and 2.63 g glucose only. As shown in the figure, the difference between these two spectra arises from their intensity backgrounds; the spectrum for the acidified solution has a higher intensity background as compared to the spectrum for the non-acidified solution, except in the region 3000-3500 cm^{-1}. The Raman peak at 3000-3500 cm^{-1} is due to OH stretching vibration in the solution, whereas the decrease of this peak height for the acidified solution is due

the presence of H^+ ions (from HCl), which interfere with oxygen atoms in the solution.

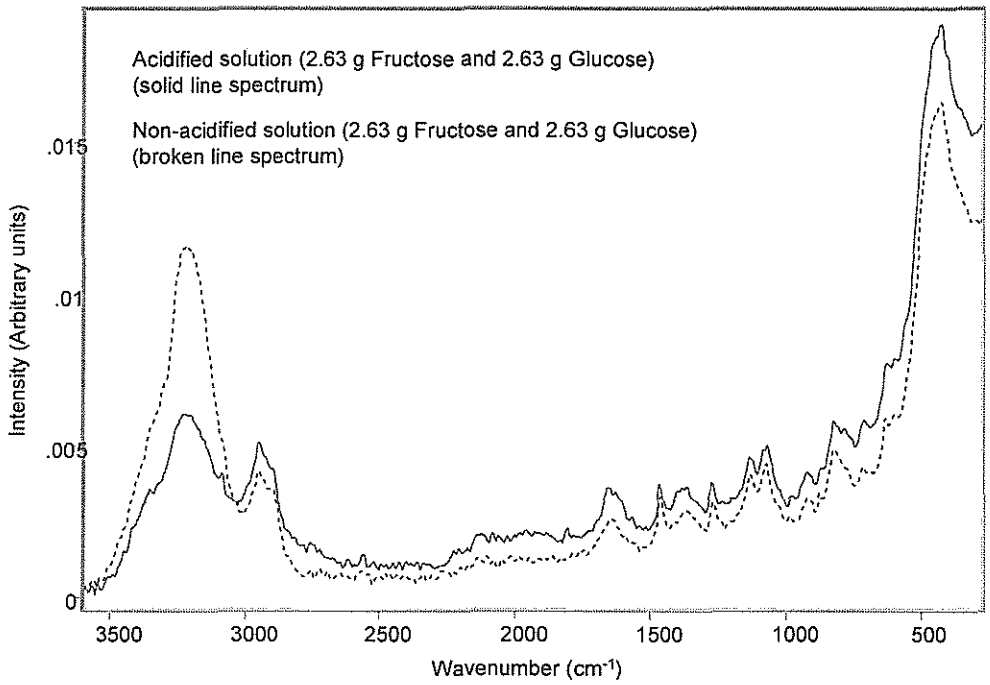

Figure 3.4 FT-Raman spectrum of acidified solution (solid line) and spectrum of non-acidified solution (broken line) of 2.63 g fructose and 2.63g glucose. The acidified spectrum has a strong intensity background as compared to the other spectrum.

In Figure 3.5, two sets of FT-Raman spectra are placed next to each other, the set above was obtained from calibration solutions and the set below, as an example, was obtained from the reaction between 20 mL solution of 20 % (w/v) sucrose and 20 mL solution of 4.0424 M HCl. As it is clearly shown in this figure, these two sets of spectra are similar, in particular their spectral changes and peak shapes; all reactions in the inversion of sucrose using several concentrations of the acid showed a similar spectral trend and peak shape.

The spectral range where Raman peaks change as sucrose decomposes into fructose and glucose are clearly observed at 685-885 cm^{-1}, as shown in Figures 3.5 and 3.6; Figure 3.6 is a three dimensional representation of the selected range shown in Figure 3.5. The three dimensional figure clearly shows how spectral peaks vary from the first (SUC4M00) to the last (SUC4M59) spectrum; some of peaks heights are increasing or decreasing with respect to the sample number. The spectral peak at 836 cm^{-1}, which can be assigned to C–H stretching vibration, decreases as sucrose molecules decompose. The C–H stretch for pure honey[81] has been observed at 866 cm^{-1}, for glucose molecules[96,100] it was observed at different Raman peaks: 860 and 836 cm^{-1}, and the spectral peak[101] at 840 cm^{-1} was assigned to the combination of CH–H stretch and CH_2 deformation.

The four spectral peaks at 706, 743, 822 and 870 cm^{-1} are for the formation of fructose and glucose. The Raman peaks at 706 and 743 cm^{-1} can be assigned to C–C–O bending vibrations because they are close to peaks observed at 710 cm^{-1} (for glucose molecules)[101] and 746 cm^{-1} (for sucrose molecules)[80]. For sugar molecules, the spectral peaks for the C–O stretching, C–C–O bending and O–C–O bending vibrations have been observed[80,101] at 715 cm^{-1}, which is close to 706 cm^{-1}. The spectral peak at 822 cm^{-1} is due to C-OH stretch[80]. The quantitative analysis of the inversion of sucrose is based on these changes.

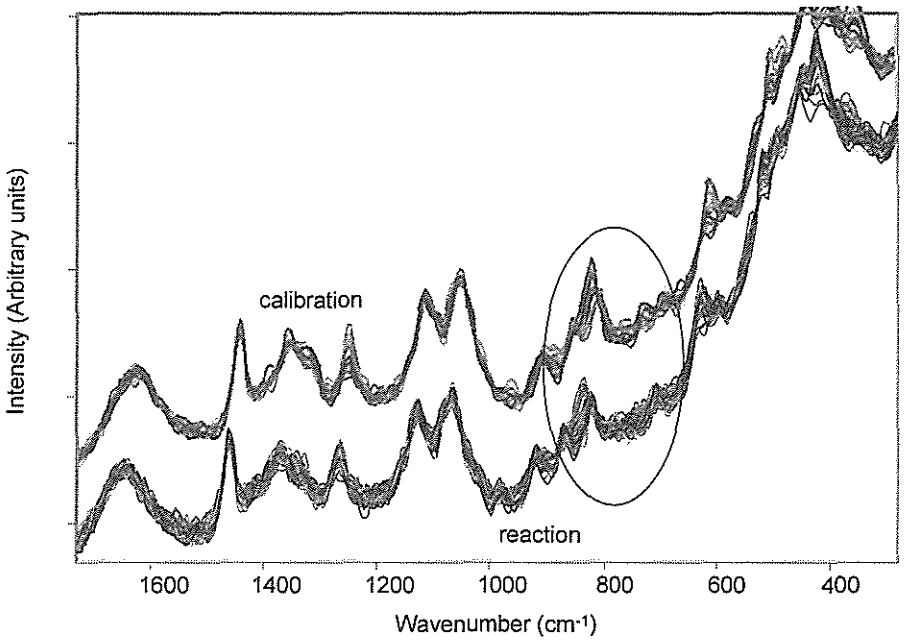

Figure 3.5 FT-Raman spectra of the calibration solutions (above) and of the reaction between 20 % (w/v) of sucrose and 4.0424 M HCl (below).

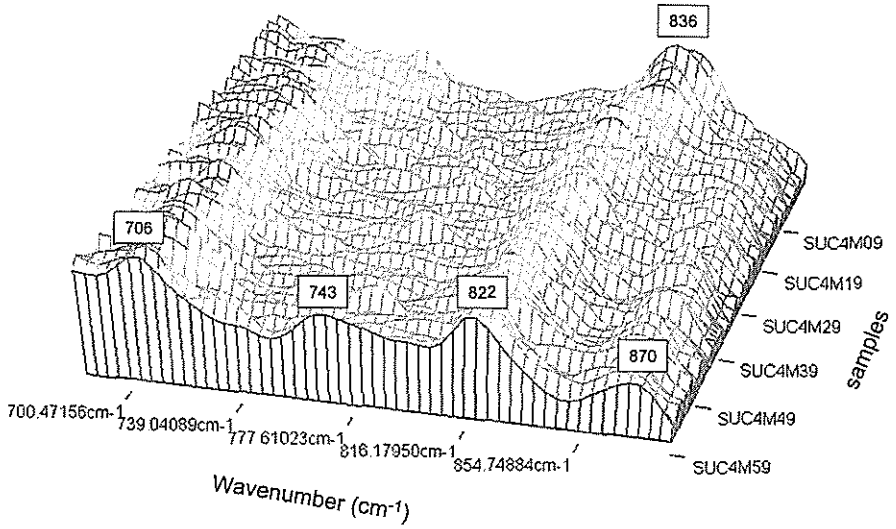

Figure 3.6 The 3-dimension FT-Raman spectra of the acid catalysed inversion of sucrose, the circled range shown in Figure 3.5 (bottom spectra; reaction spectra).

3.3.2 Results of calibration

The PLS-MDA model (the calibration method) for the prediction of mole ratios of the inversion of sucrose molecules in this work was created using the Raman spectra of mixtures of sucrose, fructose and glucose, and their mole ratios (refer to Table 3.2 and Figure 3.5 above). The regression line for sucrose mole ratios for one PC is shown in Figure 3.7 below (with coefficient of multiple determinations of 0.9767); the regression lines for fructose and glucose mole ratios for the same PC are similar to the one of sucrose. The number of samples in the regression line as shown in the figure is twice the prepared solutions for the calibration method because each solution was scanned twice to reproduce spectral data. The PLS model was checked by predicting the mole ratios of the calibration solution (see Table 3.3 below).

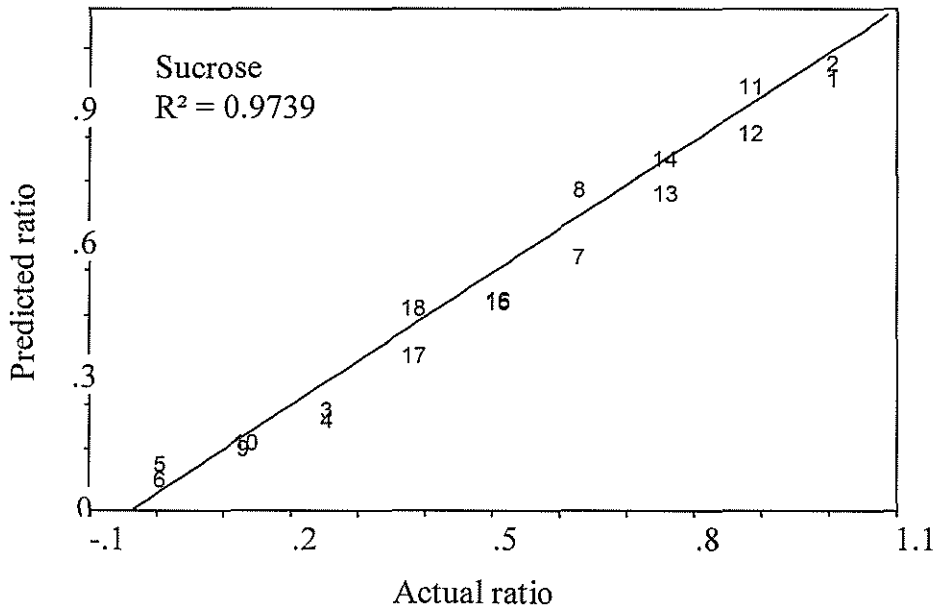

Figure 3.7 Plot of predicted versus actual mole ratio for sucrose molecules.

Table 3.3 shows the accuracy (in percentage error) and the reproducibility of sucrose, fructose and glucose concentrations in the calibration solutions. The percentage errors for sucrose in sample number 4 and for fructose and glucose in sample number 8, 11 and 12 are very large; the reproducibility of the above mentioned samples is poor. A reason for these shortcomings is due to spectra with small overlapping peaks (as shown earlier in Figures 3.4 and 3.5) and the noise in region that was analysed; a slight change in a spectral peak contributes towards a large error of error and reproducibility.

Table 3.3 Actual and predicted mole ratio of sucrose, fructose and glucose from PLS calibration, using the principal component of one.

Sample number	Actual sucrose	Predicted sucrose	% Error	Actual Fructose	Predicted Fructose	% Error	Actual Glucose	Predicted Glucose	% Error
1	1.0004	0.9464	5.39						
2	1.0004	0.9880	1.24						
3	0.2502	0.2206	11.81	0.3945	0.4100	3.94	0.3945	0.4100	3.94
4	0.2502	0.1883	24.73	0.3945	0.4270	8.25	0.3945	0.4270	8.25
5				0.5261	0.4865	7.52	0.5260	0.4866	7.50
6				0.5261	0.4997	5.02	0.5260	0.4997	5.00
7	0.6250	0.5632	9.89	0.1974	0.2299	16.44	0.1973	0.2299	16.51
8	0.6250	0.7171	14.74	0.1974	0.1489	24.59	0.1973	0.1489	24.55
9	0.1250	0.1308	4.66	0.4603	0.4573	0.65	0.4604	0.4573	0.68
10	0.1250	0.1348	7.82	0.4603	0.4552	1.10	0.4604	0.4552	1.13
11	0.8750	0.9341	6.75	0.0656	0.0348	46.96	0.0656	0.0348	46.97
12	0.8750	0.8478	3.11	0.0656	0.0802	22.23	0.0656	0.0802	22.22
13	0.7502	0.7115	5.16	0.1315	0.1518	15.46	0.1315	0.1518	15.46
14	0.7502	0.7826	4.32	0.1315	0.1144	12.99	0.1315	0.1144	13.00
15	0.5003	0.4686	6.34	0.2630	0.2796	6.32	0.2631	0.2796	6.28
16	0.5003	0.4597	8.12	0.2630	0.2843	8.09	0.2631	0.2843	8.05
17	0.3751	0.3447	8.10	0.3288	0.3448	4.86	0.3288	0.3448	4.86
18	0.3751	0.4477	19.35	0.3288	0.2906	11.62	0.3288	0.2906	11.62

The regression lines mentioned above were also used to predict mole ratios of each Raman spectrum and their values for each inversion reaction are plotted in Figure 3.8. An exponential curve was fitted to the plotted points. At higher concentrations of hydrochloric acid the exponential function does not fit sucrose data well as compared to lower concentrations, in particular when an acid concentration of ~3 M or less is used (refer to Figure 3.8, plots A–C). The pseudo-first order rate constants for plots D to F were estimated using points from measurement of concentrations at most 48 minutes because in the 48^{th} minute the signal-to-noise ratio starts to be low. The coefficient of the variable in the exponential function is taken as the pseudo first order rate constant (k_1), while the second order rate constant (k_2) is calculated according to equation 3.3; the graphical representation of rate constants will be shown later.

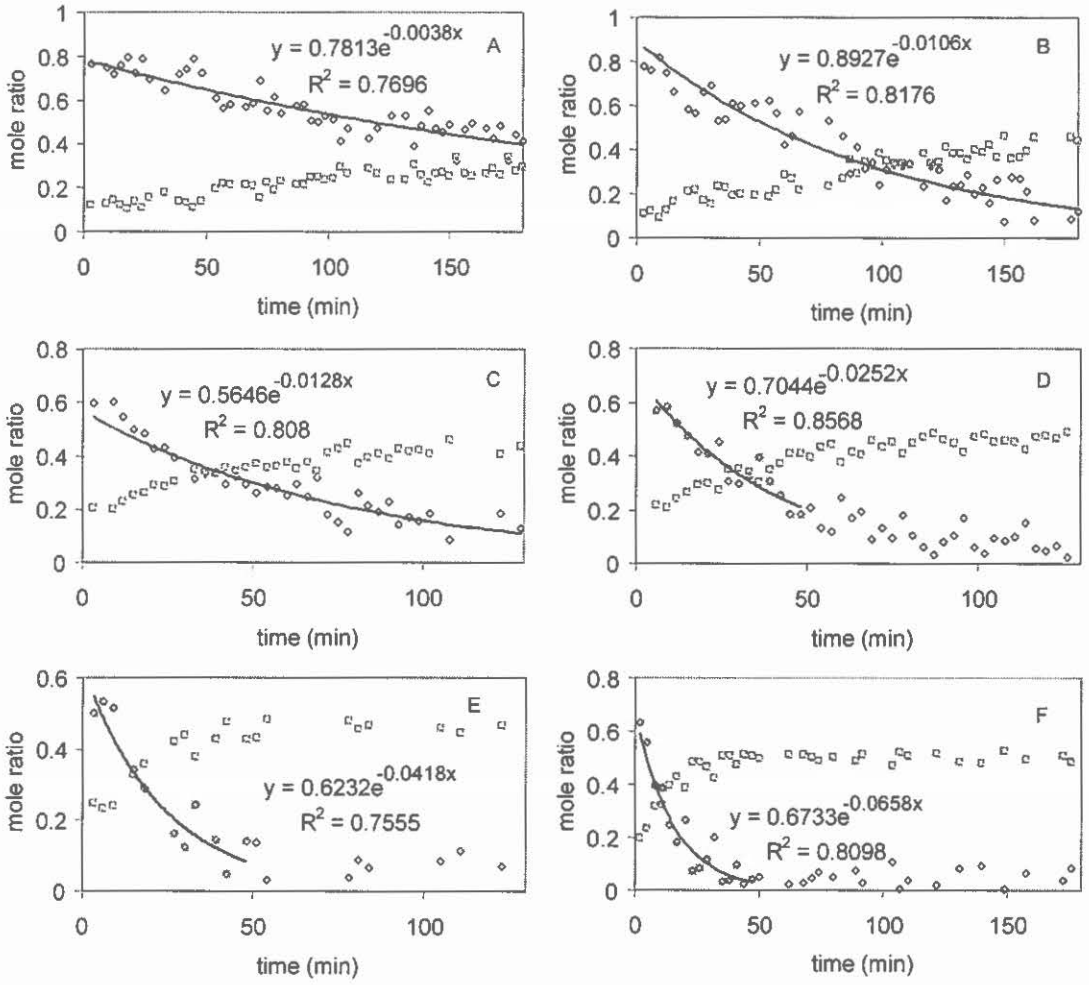

Figure 3.8 Plots of mole ratio versus time for the reaction between 20 % (w/v) sucrose (◆) and various concentrations of HCl: 1.0106 (A), 2.0212 (B), 3.0318 (C), 4.0424 (D), 5.0530 (E) and 6.1200 M (F), using the calibration method. The change of Fructose and/or glucose concentrations are shown by squares (□).

3.3.3 Results of kinetic modelling

Table 3.4 shows the PLS results for the developed FT-Raman techniques. To compare results, the same Raman spectra of the inversion of sucrose that were used in the calibration method were also used to estimate pseudo-first order rate constants using the kinetic modelling. The ranges of estimated pseudo-first order rate constants are found in the first column of each sample data in the table (also graphically represented in Figure 3.9) whereas optimised pseudo-first order rate constants are found in last column for each reaction.

The optimised rate constants were estimated using the procedure described earlier (refer to section 3.1.3). These pseudo-first order rate constants computed with one PC are shown in the table. One PC is evident, possibly because there is a strong correlation between the sucrose molecules which disappeared during the reaction and the formation of fructose and glucose molecules. For the purpose of checking the accuracy of the model, a root mean square deviation (RMSD) of experimental to theoretical values and prediction bias were calculated; for all rate constant (k) in all reactions (samples), RMSD was found to be less than 0.1 and the prediction bias was found to be less than 0.01.

Tables 3.4 PLS results of reactions between 20 % (w/v) sucrose and various concentrations of HCl molecules; acid concentrations for sample 1 to 6 are as follows: 1.0106, 2.0212, 3.0318, 4.0424, 5.0530, and 6.1200 M HCl.

Sample 1	k	PC	Prediction Bias	PRESS	R^2	RMSD	$k_{1,opt}$
	0.001	1	6.2311E-05	0.0260	0.7675	0.0226	4.3434E-03
	0.0017	1	1.2041E-04	0.0657	0.7698	0.0359	
	0.0024	1	1.8775E-04	0.1148	0.7716	0.0474	
	0.0031	1	2.6231E-04	0.1687	0.7728	0.0575	
	0.0038	1	3.4238E-04	0.2244	0.7735	0.0663	
	0.0045	1	4.2648E-04	0.2798	0.7736	0.0741	
	0.0052	1	5.1335E-04	0.3338	0.7732	0.0809	
	0.0059	1	6.0190E-04	0.3856	0.7723	0.0870	
	0.0066	1	6.9123E-04	0.4350	0.7709	0.0924	
Sample 2		PC	Prediction Bias	PRESS	R^2	RMSD	$k_{1,opt}$
	0.003	1	3.2348E-05	0.0595	0.9133	0.0352	5.4238E-03
	0.0039	1	9.5113E-05	0.0853	0.9150	0.0422	
	0.0048	1	1.7296E-04	0.1110	0.9159	0.0481	
	0.0057	1	2.6200E-04	0.1362	0.9160	0.0533	
	0.0066	1	3.5901E-04	0.1607	0.9154	0.0579	
	0.0075	1	4.6134E-04	0.1849	0.9140	0.0621	
	0.0084	1	5.6685E-04	0.2088	0.9119	0.0659	
	0.0093	1	6.7378E-04	0.2327	0.9092	0.0696	
	0.0102	1	7.8073E-04	0.2567	0.9058	0.0731	

Sample 3		PC	Prediction Bias	PRESS	R^2	RMSD	$k_{1,opt}$
	0.005	1	-1.3782E-04	0.0069	0.8910	0.0207	9.4256E-03
	0.007	1	-1.3530E-04	0.0121	0.8917	0.0276	
	0.009	1	-1.0701E-04	0.0182	0.8919	0.0337	
	0.011	1	-5.7021E-05	0.0247	0.8918	0.0393	
	0.013	1	1.1084E-05	0.0315	0.8913	0.0444	
	0.015	1	9.4135E-05	0.0385	0.8904	0.0491	
	0.017	1	1.8933E-04	0.0456	0.8891	0.0534	
	0.019	1	2.9421E-04	0.0527	0.8875	0.0574	
	0.021	1	4.0661E-04	0.0598	0.8854	0.0611	
Sample 4		PC	Prediction Bias	PRESS	R^2	RMSD	$k_{1,opt}$
	0.01	1	-1.5052E-03	0.0587	0.8465	0.0606	1.8981E-02
	0.0125	1	-1.4854E-03	0.0620	0.8468	0.0623	
	0.015	1	-1.4594E-03	0.0652	0.8470	0.0639	
	0.0175	1	-1.4278E-03	0.0683	0.8471	0.0653	
	0.02	1	-1.3910E-03	0.0713	0.8471	0.0667	
	0.0225	1	-1.3494E-03	0.0741	0.8470	0.0681	
	0.025	1	-1.3035E-03	0.0769	0.8468	0.0693	
	0.0275	1	-1.2536E-03	0.0795	0.8465	0.0705	
	0.03	1	-1.2002E-03	0.0821	0.8462	0.0716	

Sample 5		PC	Prediction Bias	PRESS	R^2	RMSD	$k_{1,opt}$
	0.03	1	-5.0951E-03	0.1473	0.7592	0.0991	4.3290E-02
	0.0325	1	-5.1592E-03	0.1550	0.7616	0.1017	
	0.035	1	-5.1949E-03	0.1617	0.7634	0.1038	
	0.0375	1	-5.2061E-03	0.1676	0.7648	0.1057	
	0.04	1	-5.1959E-03	0.1728	0.7657	0.1073	
	0.0425	1	-5.1673E-03	0.1773	0.7661	0.1087	
	0.045	1	-5.1229E-03	0.1814	0.7660	0.1100	
	0.0475	1	-5.0649E-03	0.1850	0.7654	0.1110	
	0.05	1	-4.9955E-03	0.1882	0.7644	0.1120	
Sample 6		PC	Prediction Bias	PRESS	R^2	RMSD	$k_{1,opt}$
	0.0525	1	2.1961E-03	0.0751	0.9181	0.0708	5.9980E-02
	0.05375	1	2.3265E-03	0.0751	0.9188	0.0707	
	0.055	1	2.4563E-03	0.0751	0.9193	0.0708	
	0.05625	1	2.5854E-03	0.0752	0.9197	0.0708	
	0.0575	1	2.7137E-03	0.0753	0.9200	0.0709	
	0.05875	1	2.8412E-03	0.0755	0.9201	0.0709	
	0.06	1	2.9676E-03	0.0757	0.9202	0.0711	
	0.06125	1	3.0931E-03	0.0760	0.9201	0.0712	
	0.0625	1	3.2173E-03	0.0764	0.9200	0.0714	

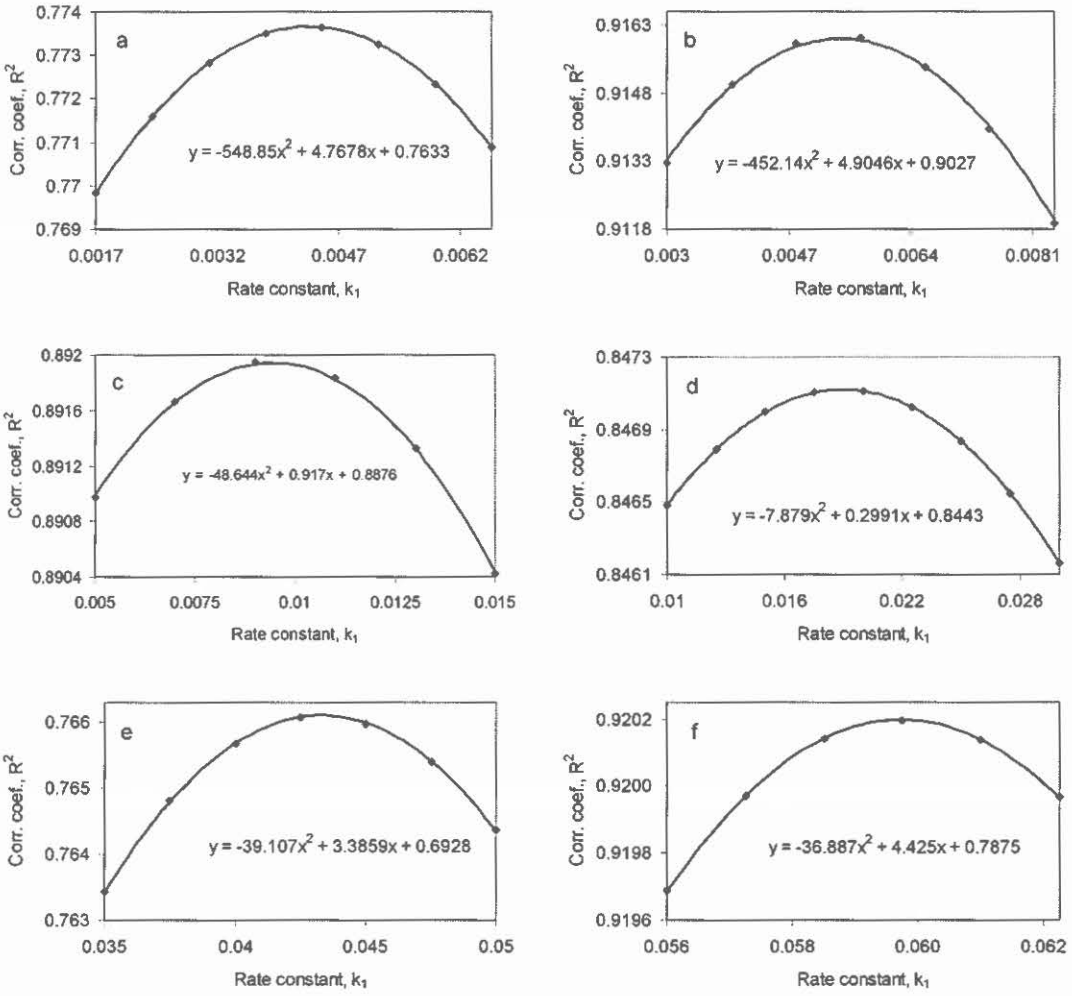

Figure 3.9 Plots of correlation coefficient (R^2) versus pseudo-first order rate constant (k_1) for the reaction between 20 % (w/v) sucrose and various concentrations of HCl: 1.0106 (a), 2.0212 (b), 3.0318 (c), 4.0424 (d), 5.0530 (e) and 6.1200 M (f).

3.3.4 Rate constants of sucrose inversion at various $[H^+]_0$ values

Rate constants of the acid catalysed inversion of sucrose molecules estimated using the calibration method and the kinetic modelling are compared in Table 3.5, Figures 3.10 and 3.11. Part 'a' in the table comprises the experimental results of this work estimated using the calibration and kinetic modelling, whereas parts 'b' and 'c' comprise the literature values obtained using polarimetry[35] (a) and attenuated total reflectance infrared (ATR-IR) spectroscopy[36] (b).

For each concentration of HCl in the table, values of rate constants (k_1 or k_2) estimated using the kinetic modelling and calibration method are comparable. In this case, the calibration method has been able to validate the kinetic modelling. Furthermore, rate constants in this work (as shown in the table) are also comparable to values found in the literature. These outcomes show that FT-Raman techniques can be used for kinetic measurements.

Figure 3.10 and 3.11 show plots of pseudo first order and second order rate constants versus concentrations of hydrogen ion ($[H^+]_0$), respectively. In these figures, cal. refers to calibration and km refers to kinetic modelling. The pseudo first order rate constants and concentrations of the hydrogen ion are exponentially related, this means that the inversion of sucrose occurs more rapidly when higher concentrations of HCl are used. The second order rate constants increase gradually as more concentrated HCl is involved in reactions, which makes the second order rate constant to be a function of the concentration of the acid.

Table 3.5 Pseudo-first order and second order rate constants for the acid catalysed inversion of sucrose molecule; experimental values: a; and literature values: b (rate constants deduced from a graph)[35] and c[36]. $[H^+]_0$ is the initial acid concentration ($mol.L^{-1}$), and rate constants: k_1 (min^{-1}) and k_2 ($L.mol^{-1}.min^{-1}$).

a	Calibration Method		Kinetic Modelling Method	
$[H^+]_0$	k_1	k_2	k_1	k_2
0.5053	3.7620E-03	7.4451E-03	4.3434E-03	8.5958E-03
1.0106	1.0564E-02	1.0453E-02	5.4238E-03	5.3669E-03
1.5159	1.2689E-02	8.3706E-03	9.4256E-03	6.2178E-03
2.0212	2.5191E-02	1.2463E-02	1.8981E-02	9.3909E-03
2.5265	4.1760E-02	1.6529E-02	4.3290E-02	1.7134E-02
3.0600	6.5811E-02	2.1507E-02	5.9980E-02	1.9601E-02
b				
0.2500	1.4000E-03	5.6000E-03		
0.5000	3.2000E-03	6.4000E-03		
1.0000	6.2000E-03	6.2000E-03		
1.5000	1.4000E-02	9.3333E-03		
2.0000	2.3000E-02	1.1500E-02		
c				
0.5210	4.8200E-03	9.2514E-03		
0.9910	1.1120E-02	1.1221E-02		
1.8060	2.6380E-02	1.4607E-02		
2.2740	3.1560E-02	1.3879E-02		

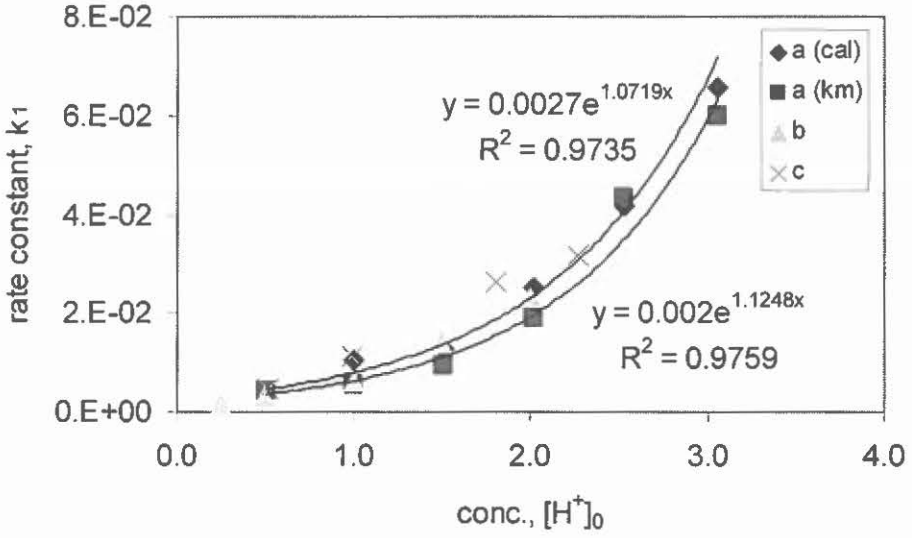

Figure 3.10 Plots of pseudo-first order rate constant (k_1) versus concentration of hydrogen ion ($[H^+]_0$) for the inversion of sucrose.

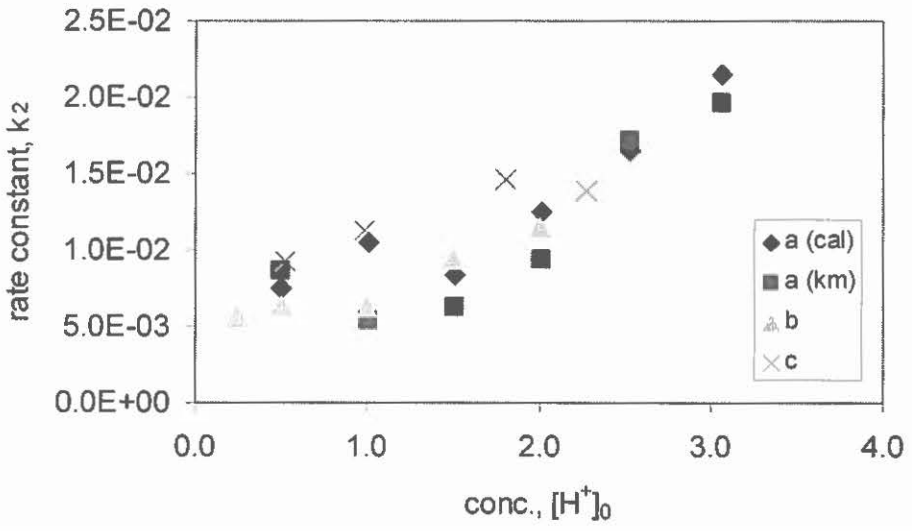

Figure 3.11 Plot of second order rate constant (k_2) versus concentration of hydrogen ion ($[H^+]_0$) for the inversion of sucrose.

3.4 Conclusions

In th.000is work, FT-Raman techniques have been successfully used to monitor the inversion of sucrose. The online system (a loop attached to a peristaltic pump that was used to circulate the reaction solution) made it possible to record spectra without changing the position of the sample and disturbing the reaction.

Though FT-Raman spectra of sucrose, fructose, glucose and their mixtures have several weak and overlapping peaks, changes of spectral peaks were monitored using multivariate data analysis. It was possible to monitor a decrease in the intensity of the Raman peak (at 836 cm^{-1}) as sucrose molecules decompose and also the increase in the intensity of Raman peaks (at 706, 743, 822 and 870 cm^{-1}) as both fructose and glucose are formed.

For kinetic studies, PLS results for the calibration method and kinetic modelling are comparable. Furthermore, the results in this work were found also comparable to literature values, in particular, the order of reaction for the inversion of sucrose and rate constants.

Therefore, the developed techniques make it feasible to quantify the hydrolysis of cobalt(III) nitrophenylphosphate complexes using multivariate data analysis. This will be the subject of the following chapter, which is the main objective of this research work.

CHAPTER 4

Cobalt(III)-assisted hydrolysis of *p*-nitrophenylphosphate

4.1.1 Introduction

The hydrolysis of *p*-nitrophenylphosphate (PNPP) using the bis-(1,3-diaminopropane)aquahydroxocobalt(III) ion ($[Co(tn)_2(OH)(H_2O)]^{2+}$) is a second order[13,15,102] reaction in aqueous media, that is, in excess water molecules. A previous investigation[102] shows that the hydrolysis in excess cobalt(III) complex has the maximum reaction rate at pH of 7.5. Another investigation[13] shows that the hydrolysis of ratio 2:1 (of $[Co(tn)_2(OH)(H_2O)]^{2+}$:PNPP) has the maximum rate at pH 7.2. The cobalt(III) assisted hydrolysis of PNPP has been found[13] to be higher than the unassisted one by an order of magnitude of 10^4.

In this chapter, FT-Raman techniques and the partial least squares (PLS) version of multivariate data analysis (MDA) are used to estimate rate constants of the above-mentioned hydrolysis (the development of these techniques are described in Chapter 3). Prior to PNPP hydrolysis, precursors of $[Co(tn)_2(OH)(H_2O)]^{2+}$ were synthesised using procedures found in the literature[9,26,27]. The structure of the synthesised cobalt(III) complexes, $[Co(tn)_2(CO_3)]^+$ (deep red crystals), was confirmed using crystallographic methods.

For the kinetic studies of PNPP hydrolysis in this work, reactions were monitored under the following pH conditions: in the first condition

reactions were initiated at pH 7.3, and then kept constant throughout; in the second condition reactions were only initiated at pH 7.3 but not kept constant.

4.1.2 Determination of first and second order rate constants

There are different pathways[13] for the reaction between $[Co(tn)_2(OH)(H_2O)]^{2+}$ and PNPP that could be modelled by the same techniques.

Pathway 1: If the above-mentioned reaction forms negligibly small intermediates (ML) (steady-state approximation: $\frac{d[ML]}{dt} = 0$) to form product(s), it can be presented by the following equation:

$$M + L \xrightarrow{k_1} P \qquad (4.1)$$

where

M is $[Co(tn)_2(OH)(H_2O)]^{2+}$, the metal complex,
L is PNPP, the ligand,
P is PNP and cobalt(III)-phosphate, products, and
k_1 is the first order rate constant.

Then the hydrolysis rate (v) with respect to L is given by

$$v = -\frac{d[L]}{dt} = k_1[L][M] \qquad (4.2)$$

When the integration of Equation 4.2 is carried-out from time t = 0 to t = t, concentration [L] = $[L]_0$ to [L] = [L] and [M] is kept constant or is in excess, then the result becomes:

$$\frac{[L]}{[L]_0} = e^{-k_1 t} \qquad (4.3)$$

The prior knowledge of [L] to estimate k_1 is not necessary because the kinetic modelling in this work is based on mole ratios. In the literature[13] k_1 is estimated from initial concentrations just after the induction period, the same approximation will be used in this work.

Alternatively, pathway 2: In this pathway, one of three mechanisms which will be described by consecutive reactions[13] (Equation 4.4, 4.5 and 4.6) is possible.

$$M + L \overset{K_2}{\longleftrightarrow} ML \qquad (4.4)$$

$$ML \xrightarrow{k_3} P \qquad (4.5)$$

and/or

$$ML + M \xrightarrow{k_4} P \qquad (4.6)$$

where

K_2 is an equilibrium constant,

K_3 is a first order rate constant, and

K_4 is a second order rate constant.

ML is an intermediate complex

Pathway 2, Condition 1: If equation 4.5 is the rate determining step for reactions (Equation 4.4 and 4.5), then the hydrolysis rate (v) can now be written as

$$v = -\frac{d[ML]}{dt} = k_3[ML] \qquad (4.7)$$

The integration of Equation 4.7 from time t = 0 to t = t and concentration [ML] = $[ML]_0$ to [ML] = [ML] gives,

$$\frac{[ML]}{[ML]_0} = e^{-k_3 t} \qquad (4.8)$$

Pathway 2, Condition 2 (an alternative): If Equation 4.6 is the rate determining step for reactions (Equations 4.4 and 4.6), then the hydrolysis rate (v) is given by

$$v = -\frac{d[ML]}{dt} = k_4[ML][M] = k_4^*[ML] \qquad (4.9)$$

where

$$k_4 = \frac{k_4^*}{[M]} \quad \text{, and} \qquad (4.10)$$

k_4^* is the pseudo first order rate constant if [M] is constant.

Similar to Equation 4.7, the integration of Equation 4.9 gives,

$$\frac{[ML]}{[ML]_0} = e^{-k_4^* t} \qquad (4.11)$$

Pathway 2, Condition 3: If the reactions represented by Equation 4.4, 4.5 and 4.6 take place at the same rate, then Equations 4.5 and 4.6 represent the rate determining steps. Therefore,

$$v = -\frac{d[ML]}{dt} = k_3[ML] + k_4[ML][M] = k^*[ML] \qquad (4.12)$$

where

$$k^* = k_3 + k_4[M], \text{ and} \qquad (4.13)$$

k* is the pseudo first order rate constant.

The integration of Equation 4.12, under the same conditions as in Equation 4.9, gives,

$$\frac{[ML]}{[ML]_0} = e^{-k^*t} \qquad (4.14)$$

As shown in Equation 4.3, 4.8, 4.11 and 4.14, the approximation in pathway 1 and 2 could be represented by an exponential function (correlating mole ratio and rate constant and/or time). According to these equations, mole ratios would not require the knowledge of the initial concentrations. This can be ideal for the kinetic modelling (KM) that will be used for reactions in this work.

4.2 Experimental

4.2.1 Reagents

All reagents used in this work were either analytical reagents or the purest grade commercially available and were used without any further purification. Cobalt(III) complexes were not commercially available, so

they were synthesised using methods found in the literature[9,26,27]. Milli-Q water (conductance = 18 MΩ.cm) was used for all rinsing and preparations of solutions.

Bought reagents: Standard pH solutions from Anatech; sodium perchorate ($NaClO_4$) from BDH laboratory; 1,3-diaminopropane (tn), 4-nitrophenol (PNP) and 4-nitrophenylphosphate disodium hexaaqua (PNPP) from Fluka chimika; perchloric acid ($HClO_4$) from PAL chemicals; hydrogen peroxide (H_2O_2) from Rochelle chemicals; cobalt(II) nitrate hexahydrate ($Co(NO_3)_2.6H_2O$), diethyl ether, ethanol (absolute), hydrochloric acid (HCl), sodium hydroxide (NaOH), sodium hydrogen carbonate ($NaHCO_3$) and sodium nitrate ($NaNO_3$) from Saarchem (Merck); potassium perchlorate ($KClO_4$) from Sigma Aldrich.

4.2.2 Synthesis of cobalt(III) complexes

Sodium tris-(carbonato)cobaltate(III) trihydrate $Na_3[Co(CO_3)_3].3H_2O$[9,27]: 10 mL of 30 % H_2O_2 was added to 50 mL solution of 29 g $Co(NO_3)_2.6H_2O$ (pink) in 100 mL beaker. This mixture was then transferred to 400 mL beaker containing 50 mL cold slurry of 42 g $NaHCO_3$. After few minutes of stirring the reaction in 400 mL beaker, the pink colour of $Co(NO_3)_2.6H_2O$ started changing to green as $Na_3[Co(CO_3)_3].3H_2O$ was formed. The stirring was continued for one hour to complete the reaction. The olive green product was washed with water, followed by absolute ethanol, and the remaining moisture on the product was evaporated by using diethyl ether[9].

Bis-(1,3-diaminopropane)carbonatocobalt(III)perchlorate $[Co(tn)_2CO_3]ClO_4$: 6 g of liquid tn was neutralised by 6 M $HClO_4$; the acid was added

drop-wise into tn because of the vigorous reaction. The pH was monitored using an Orion 9165BN Ag/AgCl electrode attached to an Orion 410A pH meter (from Thermo Electron Corporation). The neutral solution was added to a 50 mL slurry of 15 g $Na_3[Co(CO_3)_3].3H_2O$ in a 400 mL beaker, then the mixture was stirred at 75 °C for 2 hours; the green slurry turned to deep red as $[Co(tn)_2CO_3]ClO_4$ formed. The deep red slurry was filtered through a Buchner funnel and the remaining solid product on the filter paper was washed with water. The volume of the filtrates was reduced (to approximately half of its volume) at 75 °C. Then 30 mL of saturated $KClO_4$ and deep red filtrates were mixed and transferred into 200 mL beaker for overnight cooling and crystallisation (It is not clear in literature[9,26,27] whether to add saturated $KClO_4$ before or after filtration). The structure of the deep red crystals was verified by the crystallographic method at the University of Pretoria (the Department of Chemistry, Pretoria campus, RSA) and the results will be shown later.

Conversion of carbonato to aquahydroxy species: a mass of $[(tn)_2CoCO_3]ClO_4$ (depending on the required concentration of $[(tn)_2Co(H_2O)(OH)](ClO_4)_2$, refer to Table 4.1 below) was transferred into 25 mL round bottom flask. Then a mass of $HClO_4$ (calculated from the following ratio[9]: 5 mol $HClO_4$ to 2 mol $[(tn)_2CoCO_3]ClO_4$) was added to the flask to catalyse substitution of carbonate ion by water. The carbon dioxide from the carbonate ion solution was removed by stirring the mixture in an aspirator for 20 minutes at 50 °C. The pH of the solution was then adjusted to 7.3.

4.2.3 $[Co(tn)_2(OH)(H_2O)]^{2+}$ assisted hydrolysis of PNPP

$[Co(tn)_2(OH)(H_2O)]^{2+}$ assisted hydrolysis[13] of PNPP was conducted at room temperature (21.5-22 °C) and at pH of 7.3; some of the reactions were not conducted at constant pH. The ionic strength of the solution was increased by 0.6 M $NaNO_3$. These three conditions were chosen for monitoring the hydrolysis of PNPP for three hours, that is, until the reaction had proceeded close to completion. Table 4.1 below consists of concentrations of reagents, where 20 mL of $[Co(tn)_2(OH)(H_2O)]^{2+}$ was reacted with 20 mL of PNPP.

The pH of each reagent was adjusted to 7.3 using crushed pellets of NaOH or 0.1 M HCl, and then the hydrolysis pH was maintained at 7.3 using a glass rod or needle dipped in the solutions of 0.1 M NaOH or HCl to add negligibly small amounts. For comparative study, some hydrolyses were started at pH of 7.3 and then continued without keeping the pH constant throughout. The hydrolysis pH was monitored at three minutes interval using an Orion pH meter (already described above).

The FT-Raman spectra for the hydrolysis were recorded at three minute intervals for three hours, and the rate constant for each hydrolysis was estimated using equation 4.3 (refer to theory in section 4.2) and developed techniques (refer to Chapter 3). The spectral region for PLS-MDA model was selected to be 650-1430 cm^{-1}, where changes of peaks were mostly observable. Initially the wavenumber range 1240-1400 cm^{-1}, where major changes of Raman peaks for the hydrolysis were observable, was selected but it did not include the major peak of cobalt(III) complex at 935 cm^{-1}, as it will be shown later. The selected

range compared to the whole spectrum reduces computation time and it improves computation quality. Time is reduced when sizes of spectral matrices are reduced and quality of the regression line is improved when noise in the spectra is reduced.

Table 4.1 A summary of reagents for the hydrolysis at 21.5-22 °C and I = 0.6 M $NaNO_3$. M refers to the metal-complex $[Co(tn)_2(OH)(H_2O)]^{2+}$, whereas L refers to the ligand (PNPP), $[\ ]_0$ is the initial concentration ($mol.L^{-1}$) and mon. pH refers to monitored reaction starting from pH 7.3.

Batch	Sample	$[M]_0$	$[L]_0$	pH
A	1	0.0200	0.0200	7.3
A	2	0.0240	0.0160	7.3
A	3	0.0267	0.0133	7.3
A	4	0.0286	0.0144	7.3
A	5	0.0300	0.0100	7.3
A	6	0.0267	0.0133	7.3
B	7	0.0080	0.0320	7.3
B	8	0.0133	0.0267	7.3
B	9	0.0267	0.0133	7.3
C	10	0.0320	0.0080	7.3
C	11	0.0100	0.0300	7.3
C	12	0.0200	0.0200	7.3
C	13	0.0300	0.0100	7.3
D	14	0.0100	0.0300	mon. pH
D	15	0.0120	0.0280	mon. pH
D	16	0.0160	0.0240	mon. pH
E	17	0.0200	0.0200	mon. pH
E	18	0.0240	0.0160	mon. pH
E	19	0.0267	0.0133	mon. pH

4.3 Results and discussion

Crystal Data of the synthesized $[Co(tn)_2CO_3]ClO_4$: $C_7H_{20}ClCoN_4O_7$, a monoclinic, space group $P2_1/c$, with lattice constants a = 9.5347(5) Å, b = 13.2166(7) Å, c = 12.0977(7) Å and β = 111.7730(10); V = 1415.75(13) $Å^3$, and d(calc; M = 366.65, Z = 4) = 1.720 Mg/m^3. The crystal data from this work compares to values found in literature[103,104], tables for full crystal data are given in Appendix 1.

The synthesis of $[Co(tn)_2(OH)(H_2O)]^{2+}$ precursors and PNPP hydrolysis were mainly analysed by FT-Raman techniques and will be discussed under the following topics:

1 Analysis of Raman spectra of the $[Co(tn)_2(OH)(H_2O)]^{2+}$ assisted hydrolysis of PNPP
2 Estimation of rate constants for the PNPP hydrolysis

4.3.1 Analysis of Raman spectra for the $[Co(tn)_2(OH)(H_2O)]^{2+}$ assisted hydrolysis of PNPP

Figures 4.1, 4.2 and 4.3 show spectra of $Na_3[Co(CO_3)_3].3H_2O$, $[Co(tn)_2CO_3]ClO_4$ and $Co[(tn)_2(H_2O)_2](ClO_4)_3$, respectively. The Raman peak observable at 934-935 cm^{-1} (found in the last two figures) will be discussed.

CH_2 rocking vibration from tn: The strong peak at 934-935 cm^{-1} is shown in Figures 4.2 and 4.3, which is observable when tn is coordinated to cobalt, in contrast to the spectrum of $Na_3[Co(CO_3)_3].3H_2O$ in Figure 4.1. This peak mentioned above is assigned to CH_2 rocking vibration[105,106] of the amine substituted chelating ligands, and it can be also seen in the spectra of $[Co(tn)_2(OH)(H_2O)]^{2+}$. According to the above information, the appearance of this peak can also confirm the coordination of tn to the cobalt metal, which is the only ligand (in our case) having an alkyl group.

Cis- and trans-isomerisation: In a previous investigation[107] *trans*-$[(tn)_2Co(H_2O)_2]^{3+}$ was found to isomerise rapidly to the *cis*-isomer at lower pH, that is, in acidic media at 25°C. According to the above information, the compound prepared in this work is a *cis*-isomer and its Raman spectrum is shown in Figure 4.3. The addition of NaOH in the solution minimises the high *cis-trans* isomerisation rate, and it causes the dissociation of the *cis*-isomer (Equation 4.15 and 4.16).

$$cis\text{-}[Co(tn)_2(H_2O)_2]^{3+} + H_2O \xleftrightarrow{K_1} cis\text{-}[Co(tn)_2(OH)(H_2O)]^{2+} + H_3O^+ \quad (4.15)$$

$$cis\text{-}[Co(tn)_2(OH)(H_2O)]^{2+} + H_2O \xleftrightarrow{K_2} cis\text{-}[Co(tn)_2(OH)_2]^{+} + H_3O^+ \quad (4.16)$$

where pK_1 and pK_2 at 25 °C (room temperature) and 0.5 M $NaClO_4$ are 4.78-4.98 and 6.92-7.22, respectively. The *trans*-$[(tn)_2Co(OH)(H_2O)]^{2+}$ ion has been found in basic solutions, at pH 7.5 to 9.6[102].

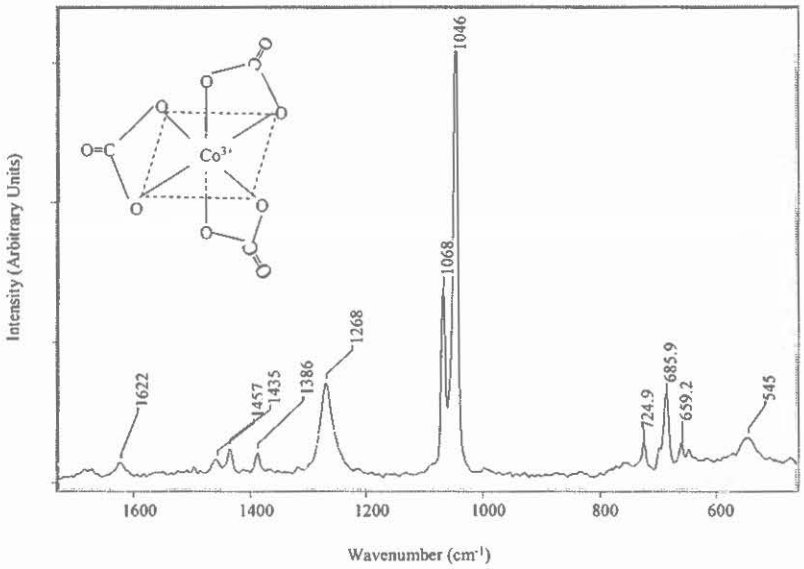

Figure 4.1 FT-Raman spectrum of solid $Na_3[Co(CO_3)_3].3H_2O$

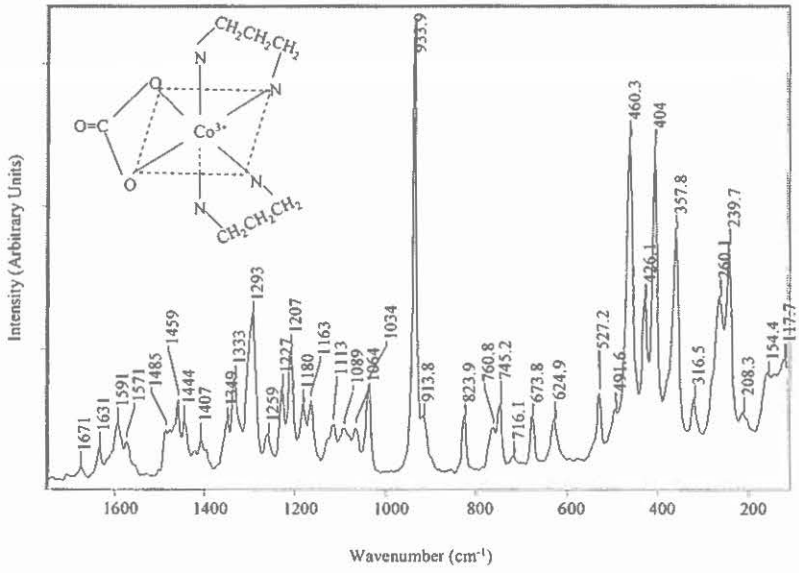

Figure 4.2 FT-Raman spectrum of solid $[(tn)_2CoCO_3]ClO_4$

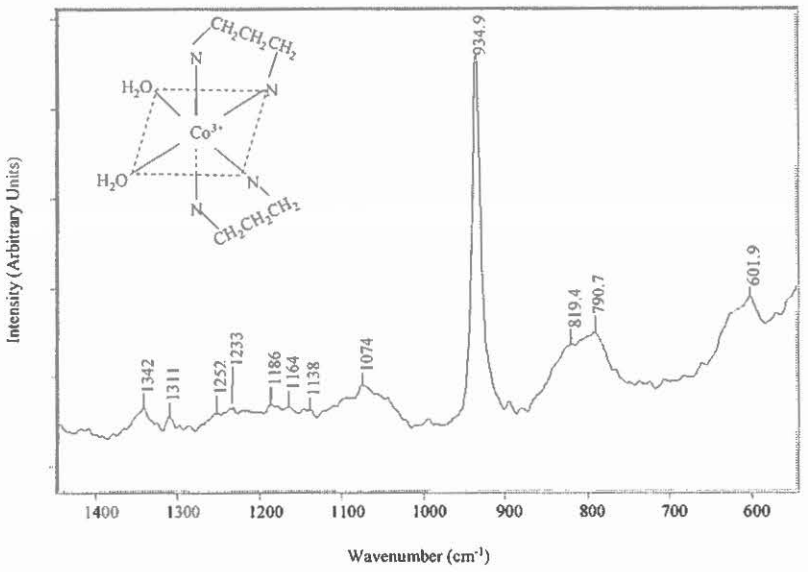

Figure 4.3 FT-Raman spectrum of the solution of 0.1 M *cis*-$[Co(tn)_2(H_2O)_2](ClO_4)_3$

Reagents and products: It is imperative to analyse FT-Raman spectra of reactants and products prior to the analysis of spectra for PNPP hydrolysis; PNP and phosphate are products of the hydrolysis. Since $[(tn)_2Co(OH)(H_2O)]^{2+}$ was used to enhance hydrolysis rates, PNPP and $[(tn)_2Co(OH)(H_2O)]^{2+}$ are reactants.

Phosphorus compounds have a P–O[108], P=O[109,110] and P–O–C (in aliphatic compounds)[30,111] stretching vibrations that can be observed at 1054-910 cm^{-1}, 1350-1150 cm^{-1} and 1050-970 cm^{-1}, respectively. FT-Raman spectra of 0.1 M PNPP and 0.1 M PNP as shown in Figure 4.4 have both similar and isolated peaks; isolated peaks were used for the monitoring of PNPP hydrolysis. Because the peaks at 982 and 737 cm^{-1} (assigned to the phosphate ion[108-112]) are very weak, only peaks at 1290 and 1266 cm^{-1} were used to estimate rate constants. As shown in Figure 4.5 below, the FT-Raman spectrum for the $[(tn)_2Co(OH)(H_2O)]^{2+}$ ion has

a strong peak at 935 cm^{-1}, which does not interfere with other peaks of interest discussed above.

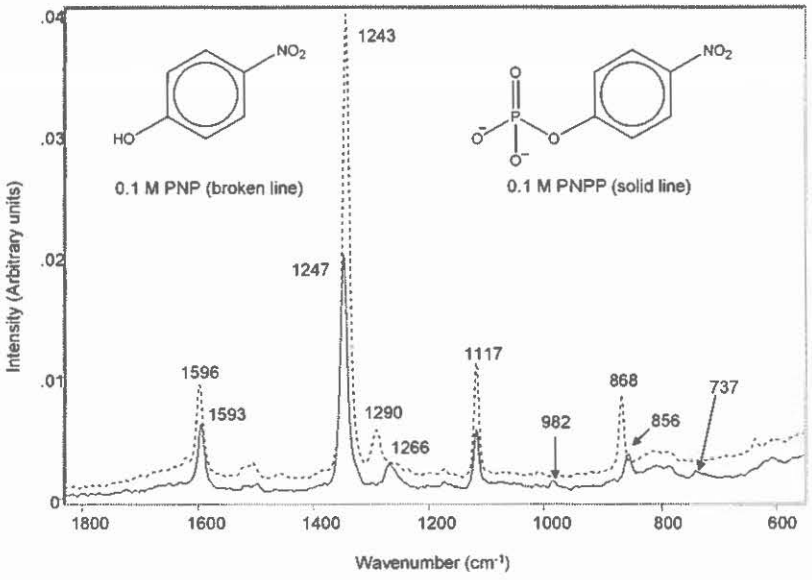

Figure 4.4 FT-Raman spectra of solutions of pure 0.1 M PNP and pure 0.1 M PNPP

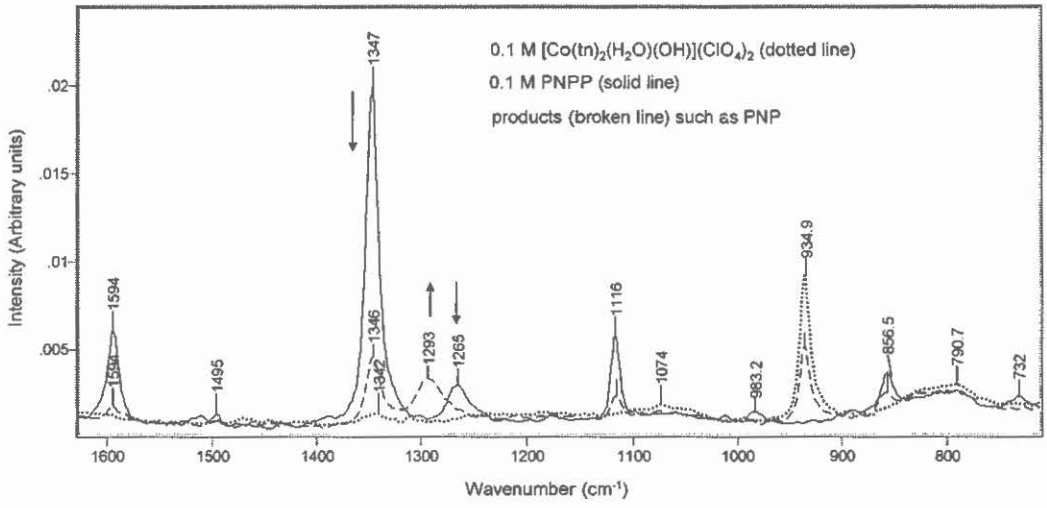

Figure 4.5 FT-Raman spectra of reagents and products in the $[Co(tn)_2(OH)(H_2O)]^{2+}$ assisted hydrolysis of PNPP. The reaction was conducted in a solution of 0.6 M $NaNO_3$.

$[Co(tn)_2(OH)(H_2O)]^{2+}$ assisted hydrolysis of PNPP: This is a Lewis acid-base reaction to form PNP and the $Co(tn)_2$phosphate complex. This reaction can be monitored by a decrease in the intensity of peaks at 1347 and 1265 cm^{-1} (PNPP disintegration) and an increase in the intensity of the peak at 1293 cm^{-1} (PNP formation)(see Figures 4.5 above, 4.6 and 4.7 below). This trend of change in the intensity of peaks was observed in all reactions at the pH of 7.3 or uncontrolled pH.

Figure 4.6 shows a 3-dimensional plot of the reaction spectra at the region 650-1430 cm^{-1}. This region, as mentioned earlier, was used for the estimation of rate constants, which will be presented later. In addition to Raman peaks at 1347, 1293 and 1265 cm^{-1}, the region was extended to 650 cm-1 for the sake of incorporating peaks characterising $[Co(tn)_2(OH)(H_2O)]^{2+}$ and PO_4^{3-}.

As shown in Figure 4.7, there is a sudden decrease in the Raman peak at 1265 cm^{-1} whereas the Raman peak at 1347 cm^{-1} gradually decreases while a peak at 1293 cm^{-1} gradually increases. According to Raman peaks in this figure, the life span of PNPP in the reaction is very short whereas the formation of PNP increases with time. A possible reason for this sudden decrease of the Raman peak is the formation of the $Co(tn)_2$phosphate complex, which is not characterised by a peak at 1265.

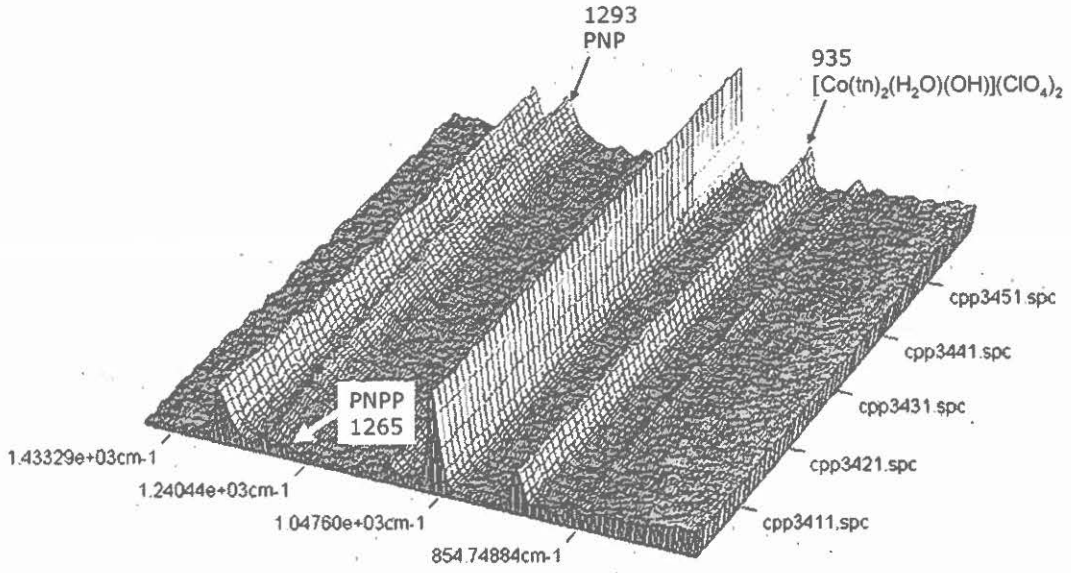

Figure 4.6 3-dimensional FT-Raman spectra for the $[Co(tn)_2(OH)(H_2O)]^{2+}$ assisted hydrolysis of PNPP in the range 650-1430 cm^{-1}.

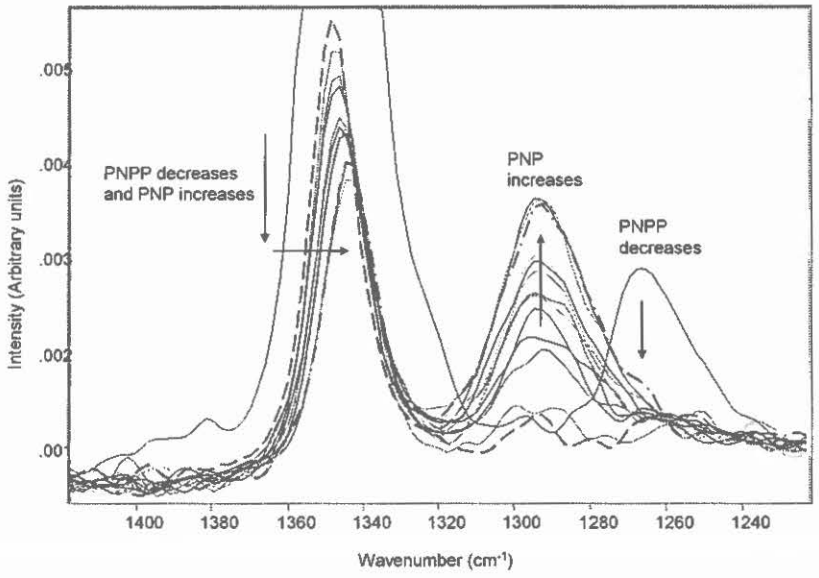

Figure 4.7 FT-Raman spectra of $[Co(tn)_2(OH)(H_2O)]^{2+}$ assisted hydrolysis of PNPP for three peaks at 1347, 1293 and 1265 cm^{-1}.

4.3.2 Estimation of rate constants for the PNPP hydrolysis

FT-Raman techniques and the procedure to estimate rate constants and also to predict mole ratio of PNPP using PLS-MDA were fully discussed in Chapter 3. The reaction between 0.0267 M $[Co(tn)_2(OH)(H_2O)]^{2+}$ and 0.0133 M PNPP (molar ratio of 2:1) will be used as an example to show plots of regression line, coefficients of multiple determination (R^2), mole ratios and pH.

Figure 4.8 is a summary of PLS-MDA results. To quantify FT-Raman spectra of this reaction, the kinetic modelling was used to create models which are represented by the regression line shown in the figure below. The rate constants were optimised using PLS-MDA and the results are presented in Figure 4.9. The rate constant of this reaction was estimated to be 1.5839×10^{-2} min^{-1}.

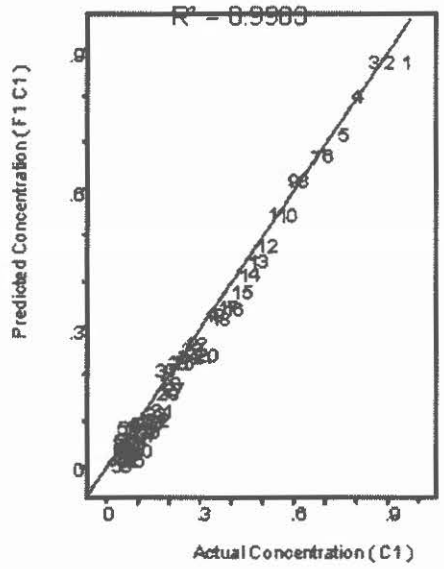

Figure 4.8 Plot of Predicted versus Actual concentrations for the molar ratio 2:1 of $Co(tn)_2PNPP$ complex.

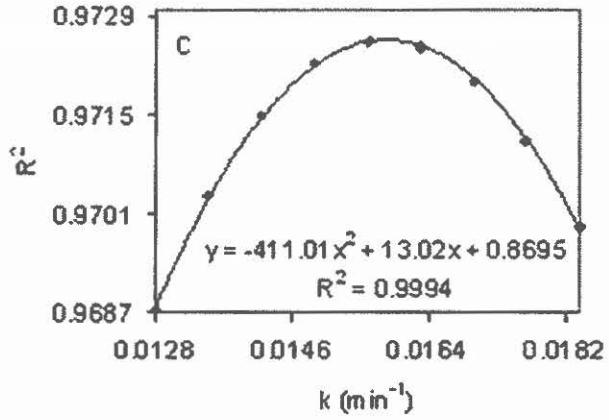

Figure 4.9 Plots of coefficient of multiple determination (R^2) versus first order rate constant ($k_{1,opt}$) for the molar ratio 2:1 of $Co(tn)_2PNPP$ complex.

Figure 4.10 below shows plots of concentrations and pH values. In this reaction, pH was initiated at 7.3 but was not kept constant throughout. When $[Co(tn)_2(H_2O)(OH)](ClO_4)_2$ and PNPP were mixed, the monitored

pH values increased to a maximum and then gradually decreased. This phenomenon was explained earlier using FT-Raman spectra (refer to section 4.3.1). The sudden increase of pH to the maximum is known as the short induction period[12]; in this work, induction period was observed at pH 8.13 in 8.00 minutes for molar ratio of 2:1.

According to Figure 4.10, the plot of mole ratio and time is correlated by an exponential function. The pH values of the solution after the induction period started decreasing as the number of moles of PNPP was decreasing. The $Co(tn)_2PNPP$ complex in basic media disintegrated to form acidic PNP. Prior to monitoring of these reactions, pH of $[Co(tn)_2(H_2O)(OH)](ClO_4)_2$ and PNPP were measured and were found to be 2.84 (due to $HClO_4$ used in the preparation) and 8.20, respectively. A reason for the pH increase will be discussed later.

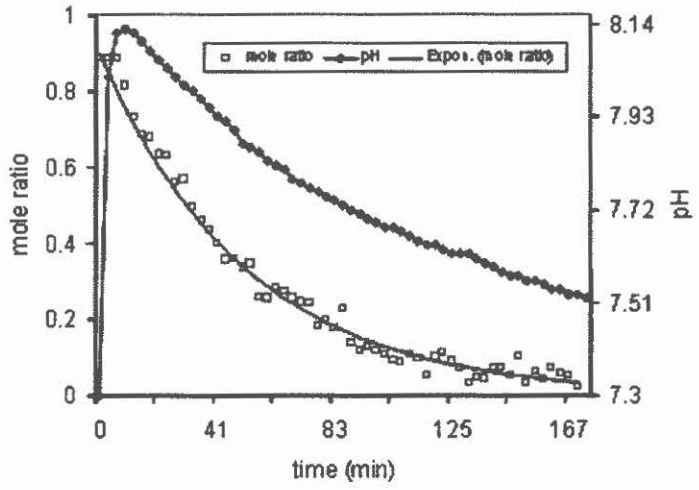

Figure 4.10 Plots of mole ratio (left ordinate) and pH (right ordinate) versus time for the ratio 2:1 of $Co(tn)_2PNPP$ complex.

Table 4.2 shows rate constants of PNPP hydrolysis at specific pH conditions (more information on rate constants can be found in Appendix 2; the rate constants in Table 4.2 were estimated using GRAMS32, which is confirmed by the Unscrambler results found in Appendix 3). The rate constants for the hydrolysis of PNPP are plotted in Figure 4.11. The rate constant (k_1) for pathway 1 or 2 are interpreted using equations already described.

Table 4.2 First order rate constants rate (k_1) of the PNPP hydrolysis with respect to PNPP estimated using FT-Raman techniques and PLS-MDA (Refer to Equations 4.2 and 4.3, and Table 4.1).

Reaction monitored at pH 7.30

Limits	$[M]_0$	$[L]_0$	[M]/[T]	k_1
	0.0200	0.0200	0.5000	9.8935E-03
	0.0240	0.0160	0.6000	8.3251E-03
	0.0267	0.0133	0.6675	1.3691E-02
	0.0286	0.0144	0.6651	1.6158E-02
	0.0300	0.0100	0.7500	8.6825E-03
	0.0267	0.0133	0.6675	1.0664E-02
	0.0080	0.0320	0.2000	5.1392E-03
	0.0133	0.0267	0.3325	8.2326E-03
	0.0267	0.0133	0.6675	8.8986E-03
	0.0320	0.0080	0.8000	7.1366E-03
	0.0100	0.0300	0.2500	6.9929E-03
	0.0200	0.0200	0.5000	8.5980E-03
	0.0300	0.0100	0.7500	1.2700E-02

Reaction monitored from pH 7.30

Limits	$[M]_0$	$[L]_0$	[M]/[T]	k_1
	0.0100	0.0300	0.2500	2.6688E-02
	0.0120	0.0280	0.3000	2.9978E-02
	0.0160	0.0240	0.4000	1.8316E-02
	0.0200	0.0200	0.5000	2.2582E-02
	0.0240	0.0160	0.6000	1.9963E-02
	0.0267	0.0133	0.6675	1.5839E-02

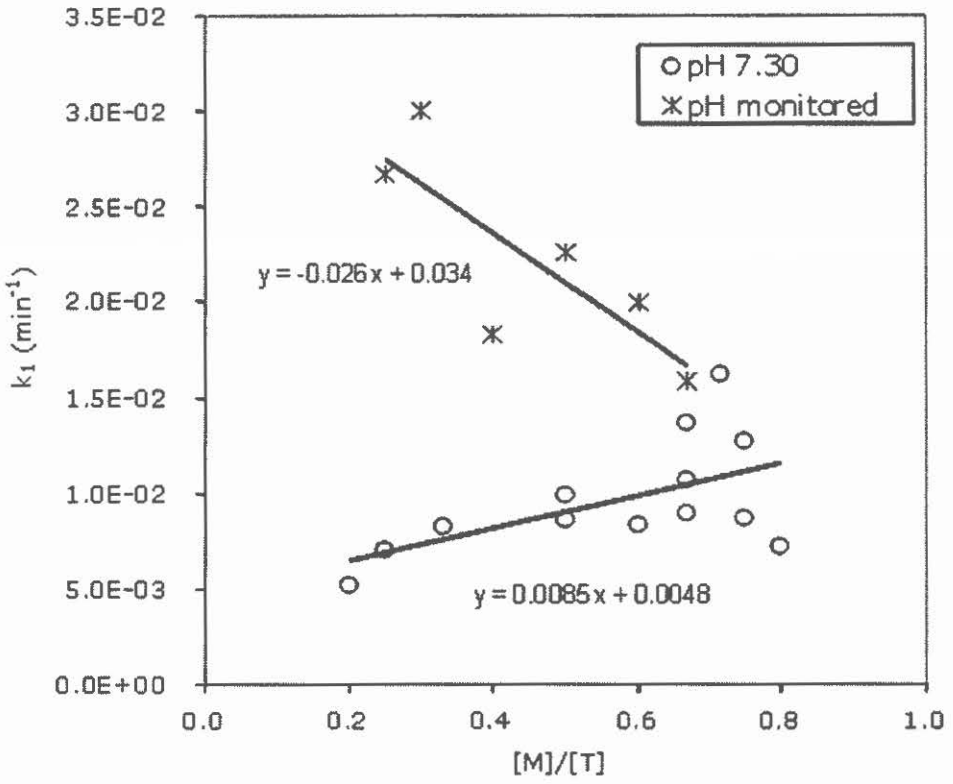

Figure 4.11 A plot of k_1 versus mole fraction of M for the hydrolysis reactions.

The discussion below is categorised into two sections; firstly the discussion focuses on the reaction scheme during the induction period and then the reaction scheme disintegration periods.

1 During the induction period

Figure 4.7 (above): Induction period is the period where the formation of PNP is very slow, which later accelerate. Sudden decrease of a Raman peak at 1265 cm^{-1} (a peak characterising PNPP) can reveal a very short life span of PNPP in the reaction, which can be attributed to the formation of the $Co(tn)_2PNPP$ complex. Although the spectrum of interest (the second spectrum)

is not clearly shown in the figure because of other spectra, it was recorded after about 5 to 6 minutes from the start of the reaction. This information will be combined with the one that will be discussed below.

Figure 4.10 (above): Mixing $[Co(tn)_2(OH)(H_2O)](ClO_4)_2$ and PNPP at pH 7.30 caused the pH of the hydrolysis to increase suddenly to a maximum of 8.16 within 5 minutes (average pH and time for several reactions). According to the pH measurement in this work, the formation of the $Co(tn)_2PNPP$ complex causes the reaction mixture to be basic, that is, releasing hydroxyl ion.

Therefore,

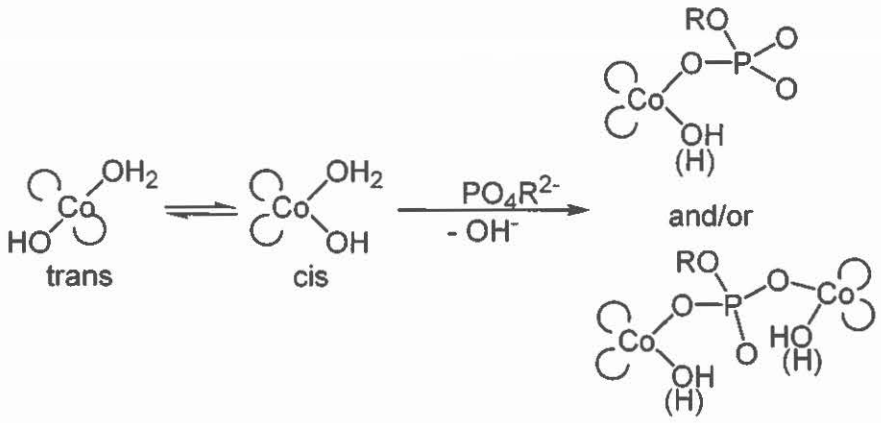

Figure 4.12 The hydrolysis scheme[13] for the formation of the $Co(tn)_2PNPP$ complex, where PNPP = PO_4R^{2-} (charges are mostly omitted).

2 During the disintegration period

Figure 4.7 (above): The disintegration period is a period where PNP is released from the complex formed above. The Raman peak at 1293 cm^{-1} (a peak characterising PNP) increases gradually as the hydrolysis proceeds. In this case, the $Co(tn)_2PNPP$ complex disintegrates to form PNP and $Co(tn)_2$phosphate complex.

Figure 4.10 (above): The $Co(tn)_2PNPP$ at the maximum pH of 8.16 for the induction period of roughly 5 minutes starts to disintegrate into acidic PNP and the $Co(tn)_2$phosphate complex. As more $O_2NC_6H_4O^-H^+$ is formed, more H^+ ions are contributed to the reaction. Hence the hydrolysis pH gradually decreases.

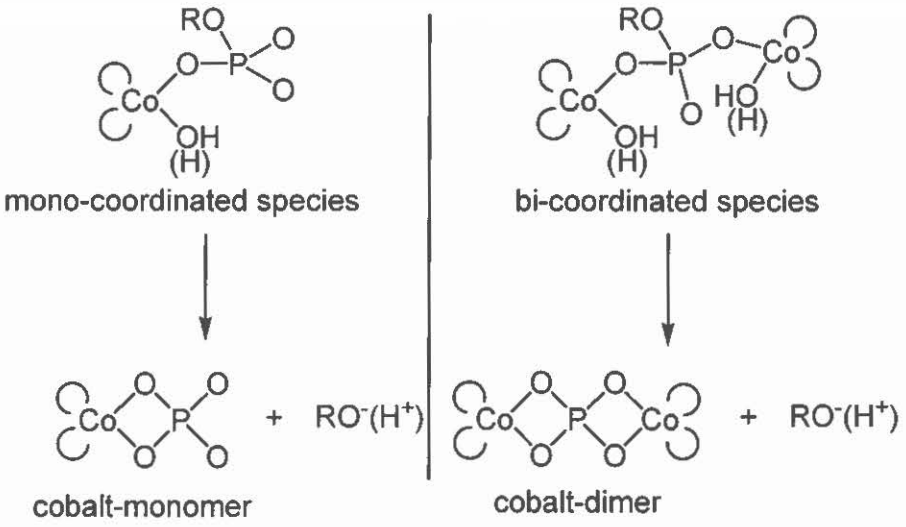

Figure 4.13 Hydrolysis scheme[13] for the disintegration of $Co(tn)_2PNPP$ complex to form ROH (PNP), in this work R = *p*-nitrophenyl (charges are mostly omitted).

4.3.3 Correlations between rate constants and hydrolysis pathways

According to the above discussions, the hydrolysis of PNPP in this work does not follow pathway 1 because of the existence of a short induction period, which is possibly caused by the formation of the $Co(tn)_2PNPP$ complex. In this section, conditions for pathway 2 (from the theory, section 4.1.2) will be discussed.

Condition 1: The first order rate constant (k_1) for each hydrolysis was estimated using the FT-Raman techniques and PLS-MDA (Table 4.3); $k_1 = k_3$ (from Equation 4.5, that is, ML $\rightarrow$ P). The rate constants from the estimated data are plotted in Figure 4.14, which is similar to Figure 4.11 above. The graph in Figure 4.11 shows plots of k_1 as a function of molar concentration of M. When points in the graph are extrapolated with a straight line, the line for the hydrolysis where pH starts at 7.3 has a negative slope; while the line for the hydrolysis at constant pH 7.3 has a positive slope. For the PNPP hydrolysis at pH 7.3, k_1 (= k_3) is scattered in the range 0.6 to 0.8 min^{-1}. The % Error in the table is calculated using the following equation below:

$$\% \text{ Error} = \left| \frac{k_1(A) - k_1(B)}{k_1(A)} \right| x100\% \qquad (4.17)$$

where

$k_1(A)$ is a first order rate constant estimated using the kinetic modelling (data in Table 4.2), and

$k_1(B)$ is a first order rate constant calculated using straight line equations found in Figure 4.14.

Table 4.3 Rate constants for PNPP hydrolysis

Reaction monitored at pH 7.30

Limits	$[M]_0$	$[L]_0$	[M]/[T]	k_1 (A)	k_1 (B)	% Error
	0.0200	0.0200	0.5000	9.8935E-03	9.0560E-03	8.47
	0.0240	0.0160	0.6000	8.3251E-03	9.9072E-03	19.00
	0.0267	0.0133	0.6675	1.3691E-02	1.0482E-02	23.44
	0.0286	0.0144	0.6651	1.6158E-02	1.0886E-02	32.63
	0.0300	0.0100	0.7500	8.6825E-03	1.1184E-02	28.81
	0.0267	0.0133	0.6675	1.0664E-02	1.0482E-02	1.71
	0.0080	0.0320	0.2000	5.1392E-03	6.5024E-03	26.53
	0.0133	0.0267	0.3325	8.2326E-03	7.6302E-03	7.32
	0.0267	0.0133	0.6675	8.8986E-03	1.0482E-02	17.79
	0.0320	0.0080	0.8000	7.1366E-03	1.1610E-02	62.68
	0.0100	0.0300	0.2500	6.9929E-03	6.9280E-03	0.93
	0.0200	0.0200	0.5000	8.5980E-03	9.0560E-03	5.33
	0.0300	0.0100	0.7500	1.2700E-02	1.1184E-02	11.94

Reaction monitored from pH 7.30

Limits	$[M]_0$	$[L]_0$	[M]/[T]	k_1 (A)	k_1 (B)	% Error
	0.0100	0.0300	0.2500	2.6688E-02	2.7497E-02	3.03
	0.0120	0.0280	0.3000	2.9978E-02	2.6196E-02	12.61
	0.0160	0.0240	0.4000	1.8316E-02	2.3595E-02	28.82
	0.0200	0.0200	0.5000	2.2582E-02	2.0994E-02	7.03
	0.0240	0.0160	0.6000	1.9963E-02	1.8393E-02	7.87
	0.0267	0.0133	0.6675	1.5839E-02	1.6637E-02	5.04

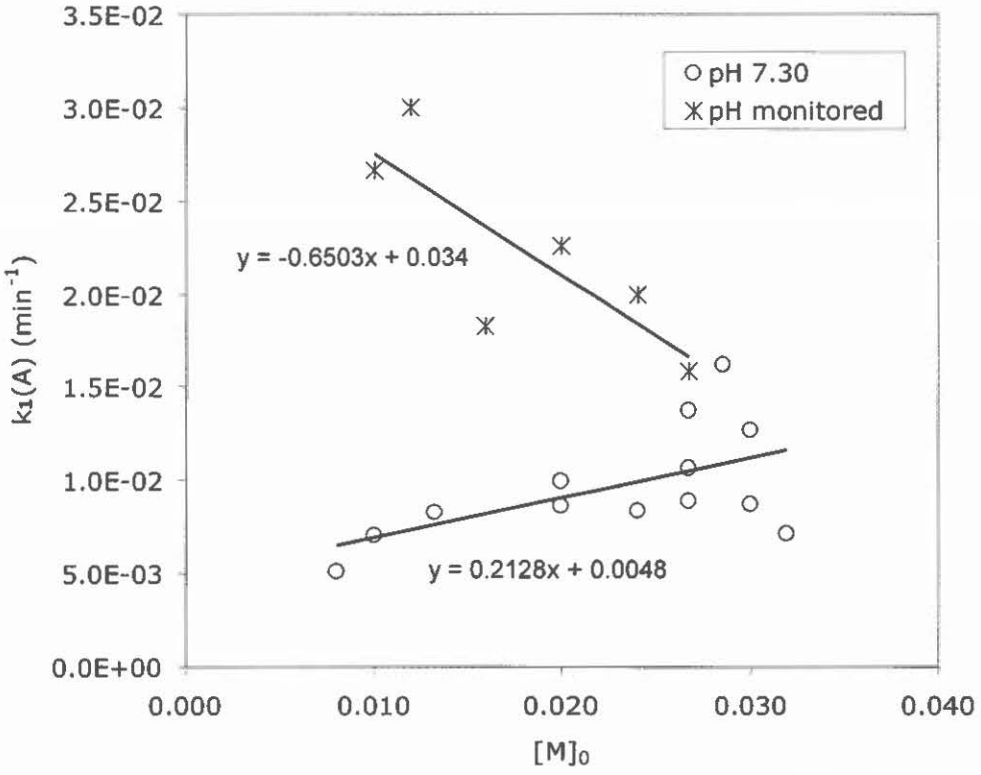

Figure 4.14 A plot of k_1 versus concentration of M for hydrolysis reactions.

Condition 2: It is an alternative to condition 1 discussed above. In this part only Equation 4.6 (that is, ML + M $\rightarrow$ P) is the rate determining step, therefore, $k_1(A) = k_4^*$ (from Equation 4.11). Since $k_1(A)$ is the first order rate constant, the second order rate constant $k_4 = k_1(A)/[M]$ (Figure 4.15). k_4 for the PNPP hydrolysis at all pH conditions decreases with a decrease in $[Co(tn)_2(OH)(H_2O)]^{2+}$, but the decrease is steeper for the hydrolysis where pH was monitored as shown in Figure 4.15 below.

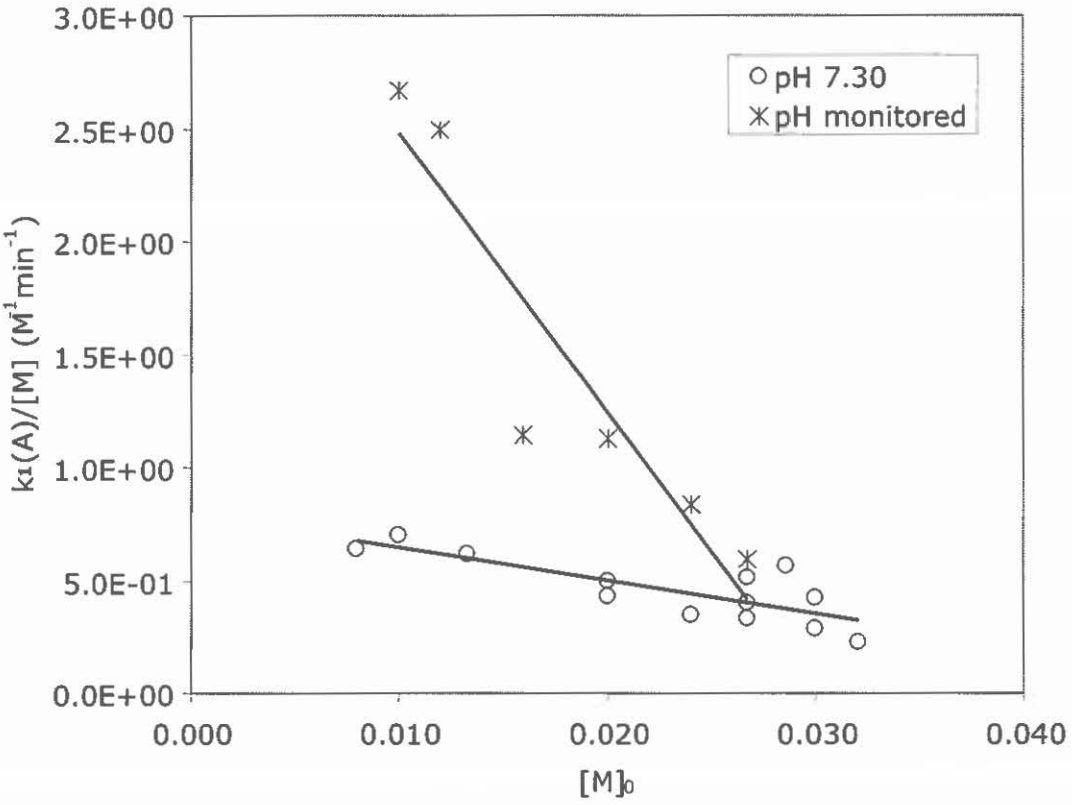

Figure 4.15 A plot of $k_1/[M]$ versus concentration of M for hydrolysis reactions.

Condition 3: It is the second alternative for condition 1, it is actually the combination of conditions 1 and 2 (Equations 4.5 and 4.6). $k_1(A) = k^*$ is pseudo first order and it is represented by the straight lines (Equation 4.18 and 4.19) from Figure 4.14.

For the PNPP hydrolysis where the pH was not kept constant,

$$k_1(A) = -0.6503[M] + 0.034 \qquad (4.18)$$

And for the hydrolysis at pH 7.3,

$$k_1(A) = 0.2128[M] + 0.0048 \qquad (4.19)$$

Therefore, it was possible to estimate different rate constants of PNPP hydrolysis using FT-Raman techniques and PLS-MDA. Hydrolysis rates were not estimated because they require the equilibrium constant, which was not determined in this work. It was possible to extract the equilibrium constant from literature, but it was only the aim of this work to estimate rate constants using the described techniques.

4.4 Conclusions

1. FT-Raman spectra were successfully used to analyse cobalt(III) complexes. Replacements of groups in cobalt(III) complexes were identified by the disappearing and appearing of spectral peaks during hydrolysis. The presence of $[Co(tn)_2(OH)(H_2O)]^{2+}$ ions during the PNPP hydrolysis was identified by a peak at 935 cm^{-1}, which is assigned to CH_2 rocking vibration of tn.

2. The Raman spectrum of $[Co(tn)_2(OH)(H_2O)]^{2+}$ has a peak 935 cm^{-1}, PNP has a peak at 1266 cm^{-1} and PNP has a peak at 1290 cm^{-1}, which overlap. The last two mentioned peaks were successfully utilised to quantify the hydrolysis of PNPP because the peak at 1266 cm^{-1} decreases as PNPP phosphate reacts while the peak at 1290 cm^{-1} increases as PNP is formed.

3. The hydrolysis of *p*-nitrophenylphosphate was conducted under two different conditions viz. at constant pH of 7.3 and an initial pH

of 7.3, which gave a graph with two different trends of rate constants. The outcome shows that first order rate constants with respect to PNPP hydrolysis are higher when the pH is not maintained throughout.

4. pH values of reactions with a changing pH from 7.3 were monitored and their change confirmed the induction period immediately after combining bis-(1,3-diaminopropane)diaqua-cobalt(III) perchlorate and *p*-nitrophenylphosphate. This phenomenon was observed by an increase of pH values from 7.3 to maximum values shown earlier (Figure 4.12), which is the coordination of the ligand (*p*-nitrophenylphosphate) to the metal complex.

CHAPTER 5

Conclusions and future investigations

5.1 Conclusions

FT-Raman techniques (a combination of online sampling system at the Raman spectrometer and kinetic modelling methods), together with the multivariate data analysis method, were successfully used to re-estimate rate constants of the hydrochloric acid catalysed inversion of sucrose. Then these techniques were used to estimate rate constants of cobalt(III) assisted hydrolysis of *p*-nitrophenyl-phosphate.

The online sampling system was achieved by making a loop that circulates the solution from the reaction vessel to the sampling compartment of the FT-Raman spectrometer, where it was scanned. The sample solution in the reaction vessel was stirred by the magnetic stirrer while a portion of the reaction solution was circulated by the peristaltic pump. This method was successfully used to conduct real time monitoring of reactions.

Though FT-Raman spectra of reaction solutions have several weak and overlapping peaks, in particular for the acid catalysed inversion of sucrose, changes of spectral peaks in general were monitored using multivariate data analysis. Considering the inversion of sucrose and the hydrolysis of cobalt(III) nitrophenylphosphate, it was possible to monitor a decrease in the intensity of the Raman peaks of reagent molecules and also the increase in the intensity of Raman peaks as products formed.

PLS results for the calibration and the kinetic modelling of the acid catalysed inversion of sucrose are comparable. The Raman spectra of sucrose, fructose and glucose, and rate constants for the inversion of sucrose were found to be comparable to the values reported in the literature. For the hydrolysis of cobalt(III) nitrophenylphosphate, it was found that rate constants where the pH is maintained at 7.30 gave results which differ from those where the pH is started at 7.30 and allowed to change during the reaction. The average rate constant for a 2:1 ($[Co(tn)_2(OH)(H_2O)]^{2+}$:PNPP) was found to be approximately 3×10^4 times the unassisted PNPP hydrolysis rate reported in the literature.

5.2 Future investigations

All reactions for the hydrolysis of cobalt(III) nitrophenylphosphate were carried-out in 8-10 x 10^{-3} M because their Raman peaks at lower concentrations such as 10^{-6} M were very weak. Real time monitoring of reactions at lower concentrations of reagents can be achieved by enhancing spectral peaks with non-reacting silver or gold colloids. The surface enhancement is possible when the Raman effect is close to the rough metal surface.

It is difficult to assign spectral peaks and to characterise the hydrolysis of cobalt(III) nitrophenylphosphate because theoretical studies for vibrational modes of p-nitrophenylphosphate and bis-(1,3-diaminopropane)diaquacobalt(III) perchlorate have not been done yet. Future uses of chemical modelling for these compounds or complexes and reactions would be an advantage to interpret experimental evidence.

APPENDICES

Appendix 1: Crystallographic data for $[Co(tn)_2CO_3]ClO_4$

Table 1. Crystal data and structure refinement for SP01.

Identification code	sp01_abs	
Empirical formula	$C_7 H_{20} Cl Co N_4 O_7$	
Formula weight	366.65	
Temperature	293(2) K	
Wavelength	0.71073 Å	
Crystal system	Monoclinic	
Space group	$P 2_1/c$	
Unit cell dimensions	a = 9.5347(5) Å	a= 90°.
	b = 13.2166(7) Å	b= 111.7730(10)°.
	c = 12.0977(7) Å	g = 90°.
Volume	1415.75(13) $Å^3$	
Z	4	
Density (calculated)	1.720 Mg/m^3	
Absorption coefficient	1.437 mm^{-1}	
F(000)	760	
Crystal size	0.42 x 0.41 x 0.16 mm^3	
Theta range for data collection	2.77 to 26.49°.	
Index ranges	-11<=h<=9, -15<=k<=12, -8<=l<=15	
Reflections collected	7336	
Independent reflections	2670 [R(int) = 0.0205]	
Completeness to theta = 25.00°	99.5 %	
Absorption correction	Semi-empirical from equivalents	
Max. and min. transmission	0.795 and 0.583	
Refinement method	Full-matrix least-squares on F^2	
Data / restraints / parameters	2670 / 0 / 218	
Goodness-of-fit on F^2	1.083	
Final R indices [I>2sigma(I)]	R1 = 0.0334, wR2 = 0.0871	
R indices (all data)	R1 = 0.0354, wR2 = 0.0894	
Extinction coefficient	0	
Largest diff. peak and hole	0.457 and -0.358 $e.Å^{-3}$	

Appendix 2: PLS-MDA results for PNPP hydrolysis using GRAMS32. Below are results of twenty one samples for the modelling of the reaction.

Sample 1	k	PC	Prediction Bias	PRESS	R^2	RMSD	$k_{1,opt}$
	0.00556	1	-0.00032	0.03749	0.93552	0.03273	0.00989
	0.00695	1	-0.00032	0.04956	0.93755	0.03763	
	0.00833	1	-0.00028	0.06125	0.93879	0.04183	
	0.00972	1	-0.00023	0.07260	0.93925	0.04554	
	0.01111	1	-0.00016	0.08378	0.93894	0.04893	
	0.01250	1	-0.00008	0.09502	0.93787	0.05210	
	0.01389	1	0.00001	0.10652	0.93607	0.05517	
	0.01528	1	0.00010	0.11845	0.93355	0.05818	
	0.01667	1	0.00020	0.13092	0.93036	0.06116	

Sample 2	k	PC	Prediction Bias	PRESS	R^2	RMSD	$k_{1,opt}$
	0.01110	1	0.00014	0.05940	0.95688	0.04120	0.01369
	0.01180	1	0.00019	0.06214	0.95751	0.04213	
	0.01250	1	0.00024	0.06486	0.95794	0.04305	
	0.01320	1	0.00029	0.06762	0.95817	0.04395	
	0.01390	1	0.00034	0.07045	0.95820	0.04486	
	0.01460	1	0.00040	0.07339	0.95804	0.04579	
	0.01530	1	0.00046	0.07647	0.95769	0.04674	
	0.01600	1	0.00051	0.07972	0.95716	0.04773	
	0.01670	1	0.00057	0.08316	0.95644	0.04874	

Sample 3	k	PC	Prediction Bias	PRESS	R^2	RMSD	$k_{1,opt}$
	0.00555	1	0.00118	0.03515	0.94677	0.03169	0.00868
	0.00642	1	0.00136	0.04259	0.94768	0.03488	
	0.00729	1	0.00153	0.05000	0.94830	0.03780	
	0.00816	1	0.00171	0.05737	0.94861	0.04049	
	0.00903	1	0.00188	0.06471	0.94864	0.04300	
	0.00990	1	0.00205	0.07203	0.94837	0.04537	
	0.01076	1	0.00221	0.07938	0.94782	0.04762	
	0.01163	1	0.00237	0.08680	0.94699	0.04980	
	0.01250	1	0.00252	0.09431	0.94588	0.05191	

Sample 4	k	PC	Prediction Bias	PRESS	R^2	RMSD	$k_{1,opt}$
	0.00100	1	0.00007	0.00154	0.94883	0.00663	0.00833
	0.00263	1	0.00020	0.00825	0.95305	0.01535	
	0.00425	1	0.00036	0.01715	0.95621	0.02214	
	0.00588	1	0.00055	0.02663	0.95830	0.02758	
	0.00750	1	0.00074	0.03620	0.95932	0.03216	
	0.00913	1	0.00095	0.04595	0.95930	0.03623	
	0.01075	1	0.00115	0.05617	0.95824	0.04006	
	0.01238	1	0.00136	0.06720	0.95618	0.04382	
	0.01400	1	0.00156	0.07930	0.95315	0.04760	

Sample 5	k	PC	Prediction Bias	PRESS	R^2	RMSD	$k_{1,opt}$
	0.00100	1	0.00006	0.00235	0.92556	0.00820	0.00274
	0.00141	1	0.00009	0.00444	0.92583	0.01126	
	0.00181	1	0.00013	0.00705	0.92603	0.01419	
	0.00222	1	0.00016	0.01010	0.92616	0.01699	
	0.00262	1	0.00020	0.01354	0.92621	0.01967	
	0.00303	1	0.00023	0.01732	0.92620	0.02224	
	0.00344	1	0.00027	0.02138	0.92611	0.02472	
	0.00384	1	0.00031	0.02569	0.92596	0.02709	
	0.00425	1	0.00035	0.03023	0.92573	0.02939	

Sample 6	k	PC	Prediction Bias	PRESS	R^2	RMSD	$k_{1,opt}$
	0.00830	2	0.00222	0.07837	0.92592	0.04732	0.01066
	0.00900	2	0.00233	0.08602	0.92601	0.04957	
	0.00970	2	0.00242	0.09337	0.92607	0.05165	
	0.01040	2	0.00250	0.10041	0.92609	0.05356	
	0.01110	2	0.00256	0.10709	0.92608	0.05531	
	0.01180	2	0.00261	0.11340	0.92604	0.05692	
	0.01250	2	0.00264	0.11934	0.92598	0.05839	
	0.01320	2	0.00265	0.12489	0.92590	0.05973	
	0.01390	2	0.00264	0.13005	0.92579	0.06096	

Sample 7	k	PC	Prediction Bias	PRESS	R^2	RMSD	$k_{1,opt}$
	0.00110	1	0.00011	0.00276	0.92823	0.00888	0.00253
	0.00141	1	0.00015	0.00439	0.92839	0.01121	
	0.00173	1	0.00018	0.00633	0.92852	0.01345	
	0.00204	1	0.00021	0.00855	0.92860	0.01563	
	0.00235	1	0.00025	0.01100	0.92864	0.01773	
	0.00267	1	0.00028	0.01367	0.92864	0.01976	
	0.00298	1	0.00032	0.01653	0.92861	0.02173	
	0.00329	1	0.00036	0.01956	0.92853	0.02364	
	0.00360	1	0.00039	0.02271	0.92841	0.02547	

Sample 8	k	PC	Prediction Bias	PRESS	R^2	RMSD	$k_{1,opt}$
	0.00582	2	-0.00014	0.01976	0.96753	0.02376	0.00714
	0.00621	2	-0.00013	0.02153	0.96777	0.02480	
	0.00661	2	-0.00013	0.02332	0.96792	0.02582	
	0.00701	2	-0.00012	0.02516	0.96799	0.02681	
	0.00741	2	-0.00012	0.02704	0.96798	0.02779	
	0.00781	2	-0.00011	0.02897	0.96788	0.02877	
	0.00820	2	-0.00010	0.03097	0.96769	0.02974	
	0.00860	2	-0.00009	0.03303	0.96742	0.03072	
	0.00900	2	-0.00007	0.03519	0.96707	0.03171	

Sample 9	k	PC	Prediction Bias	PRESS	R^2	RMSD	$k_{1,opt}$
	0.00300	2	0.00050	0.04606	0.78459	0.03628	0.00514
	0.00340	2	0.00055	0.05664	0.78487	0.04023	
	0.00380	2	0.00059	0.06780	0.78510	0.04401	
	0.00419	2	0.00063	0.07941	0.78527	0.04763	
	0.00459	2	0.00066	0.09139	0.78538	0.05110	
	0.00499	2	0.00070	0.10366	0.78543	0.05442	
	0.00539	2	0.00072	0.11614	0.78543	0.05760	
	0.00579	2	0.00075	0.12877	0.78536	0.06066	
	0.00618	2	0.00077	0.14149	0.78524	0.06358	

Sample 10	k	PC	Prediction Bias	PRESS	R^2	RMSD	$k_{1,opt}$
	0.00500	1	-0.00013	0.01930	0.96134	0.02348	0.00890
	0.00570	1	-0.00011	0.02279	0.96238	0.02552	
	0.00640	1	-0.00008	0.02625	0.96322	0.02739	
	0.00710	1	-0.00005	0.02968	0.96385	0.02912	
	0.00780	1	-0.00002	0.03311	0.96427	0.03076	
	0.00850	1	0.00002	0.03656	0.96449	0.03232	
	0.00920	1	0.00007	0.04007	0.96450	0.03384	
	0.00990	1	0.00011	0.04367	0.96431	0.03532	
	0.01060	1	0.00016	0.04740	0.96392	0.03680	

Sample 11	k	PC	Prediction Bias	PRESS	R^2	RMSD	$k_{1,opt}$
	0.00500	1	-0.00006	0.08715	0.92673	0.04990	0.00823
	0.00570	1	-0.00003	0.09260	0.92754	0.05144	
	0.00640	1	0.00001	0.09786	0.92816	0.05288	
	0.00710	1	0.00005	0.10297	0.92858	0.05424	
	0.00780	1	0.00009	0.10797	0.92879	0.05554	
	0.00850	1	0.00014	0.11290	0.92881	0.05680	
	0.00920	1	0.00018	0.11780	0.92863	0.05801	
	0.00990	1	0.00023	0.12270	0.92827	0.05921	
	0.01060	1	0.00027	0.12764	0.92771	0.06039	

Sample 12	k	PC	Prediction Bias	PRESS	R^2	RMSD	$k_{1,opt}$
	0.00010	7	0.00000	0.00001	0.95534	0.00064	0.00299
	0.00110	7	0.00002	0.00151	0.95652	0.00656	
	0.00210	7	0.00009	0.00487	0.95720	0.01179	
	0.00310	7	0.00020	0.00951	0.95739	0.01649	
	0.00410	7	0.00035	0.01513	0.95708	0.02079	
	0.00510	7	0.00054	0.02155	0.95629	0.02482	
	0.00610	7	0.00073	0.02872	0.95502	0.02864	
	0.00710	7	0.00094	0.03661	0.95329	0.03234	
	0.00810	7	0.00119	0.04523	0.95114	0.03595	

Sample 13	k	PC	Prediction Bias	PRESS	R^2	RMSD	$k_{1,opt}$
	0.00950	1	0.00039	0.20802	0.82961	0.07709	0.01270
	0.01037	1	0.00045	0.22736	0.83060	0.08060	
	0.01124	1	0.00050	0.24566	0.83127	0.08378	
	0.01211	1	0.00056	0.26296	0.83163	0.08668	
	0.01298	1	0.00062	0.27930	0.83168	0.08933	
	0.01385	1	0.00068	0.29475	0.83142	0.09177	
	0.01471	1	0.00074	0.30938	0.83086	0.09402	
	0.01558	1	0.00080	0.32327	0.83001	0.09611	
	0.01645	1	0.00086	0.33648	0.82888	0.09805	

Sample 14	k	PC	Prediction Bias	PRESS	R^2	RMSD	$k_{1,opt}$
	0.00050	1	0.00002	0.00073	0.91099	0.00456	0.00699
	0.00170	1	0.00009	0.00719	0.91363	0.01434	
	0.00290	1	0.00018	0.01806	0.91574	0.02271	
	0.00410	1	0.00028	0.03137	0.91731	0.02994	
	0.00530	1	0.00040	0.04591	0.91833	0.03622	
	0.00650	1	0.00052	0.06097	0.91882	0.04174	
	0.00770	1	0.00066	0.07614	0.91877	0.04664	
	0.00890	1	0.00079	0.09125	0.91818	0.05106	
	0.01010	1	0.00093	0.10623	0.91707	0.05509	

Sample 15	k	PC	Prediction Bias	PRESS	R^2	RMSD	$k_{1,opt}$
	0.00500	1	0.00014	0.00921	0.98167	0.01623	0.00860
	0.00600	1	0.00021	0.01119	0.98301	0.01788	
	0.00700	1	0.00028	0.01312	0.98391	0.01936	
	0.00800	1	0.00036	0.01514	0.98437	0.02080	
	0.00900	1	0.00044	0.01739	0.98440	0.02229	
	0.01000	1	0.00053	0.02001	0.98401	0.02391	
	0.01100	1	0.00062	0.02313	0.98320	0.02570	
	0.01200	1	0.00072	0.02684	0.98197	0.02769	
	0.01300	1	0.00081	0.03125	0.98034	0.02988	

Sample 16	k	PC	Prediction Bias	PRESS	R^2	RMSD	$k_{1,opt}$
	0.01550	2	0.00008	0.06853	0.98230	0.03408	0.01832
	0.01620	2	0.00012	0.06746	0.98270	0.03381	
	0.01690	2	0.00016	0.06666	0.98299	0.03361	
	0.01760	2	0.00020	0.06617	0.98316	0.03349	
	0.01830	2	0.00023	0.06601	0.98322	0.03345	
	0.01900	2	0.00026	0.06621	0.98316	0.03350	
	0.01970	2	0.00029	0.06676	0.98299	0.03364	
	0.02040	2	0.00031	0.06768	0.98271	0.03387	
	0.02110	2	0.00033	0.06894	0.98232	0.03418	

Sample 17	k	PC	Prediction Bias	PRESS	R^2	RMSD	$k_{1,opt}$
	0.01970	1	-0.00007	0.06016	0.98213	0.03221	0.02258
	0.02040	1	-0.00002	0.05576	0.98333	0.03101	
	0.02110	1	0.00003	0.05254	0.98417	0.03010	
	0.02180	1	0.00008	0.05044	0.98467	0.02949	
	0.02250	1	0.00012	0.04939	0.98485	0.02918	
	0.02320	1	0.00017	0.04935	0.98470	0.02917	
	0.02390	1	0.00021	0.05023	0.98426	0.02943	
	0.02460	1	0.00025	0.05196	0.98352	0.02993	
	0.02530	1	0.00030	0.05447	0.98250	0.03065	

Sample 18	k	PC	Prediction Bias	PRESS	R^2	RMSD	$k_{1,opt}$
	0.01280	1	-0.00003	0.11258	0.96875	0.04368	0.01584
	0.01350	1	0.00002	0.10877	0.97035	0.04294	
	0.01420	1	0.00008	0.10603	0.97151	0.04239	
	0.01490	1	0.00013	0.10447	0.97224	0.04208	
	0.01560	1	0.00018	0.10415	0.97256	0.04201	
	0.01630	1	0.00024	0.10508	0.97247	0.04220	
	0.01700	1	0.00029	0.10728	0.97199	0.04264	
	0.01770	1	0.00034	0.11070	0.97114	0.04332	
	0.01840	1	0.00039	0.11531	0.96992	0.04421	

Sample 19	k	PC	Prediction Bias	PRESS	R^2	RMSD	$k_{1,opt}$
	0.01750	1	-0.00002	0.04446	0.98822	0.02769	0.01996
	0.01820	1	0.00003	0.04052	0.98929	0.02643	
	0.01890	1	0.00009	0.03792	0.98998	0.02557	
	0.01960	1	0.00014	0.03663	0.99031	0.02513	
	0.02030	1	0.00020	0.03660	0.99029	0.02512	
	0.02100	1	0.00025	0.03778	0.98994	0.02552	
	0.02170	1	0.00030	0.04011	0.98927	0.02630	
	0.02240	1	0.00035	0.04351	0.98828	0.02739	
	0.02310	1	0.00040	0.04792	0.98701	0.02874	

Sample 20	k	PC	Prediction Bias	PRESS	R^2	RMSD	$k_{1,opt}$
	0.02700	1	0.00039	0.13567	0.96173	0.04795	0.02998
	0.02770	1	0.00043	0.13103	0.96269	0.04713	
	0.02840	1	0.00048	0.12739	0.96337	0.04647	
	0.02910	1	0.00052	0.12468	0.96379	0.04597	
	0.02980	1	0.00056	0.12283	0.96395	0.04563	
	0.03050	1	0.00060	0.12180	0.96387	0.04544	
	0.03120	1	0.00064	0.12151	0.96356	0.04538	
	0.03190	1	0.00068	0.12193	0.96303	0.04546	
	0.03260	1	0.00072	0.12298	0.96228	0.04566	

Sample 21	k	PC	Prediction Bias	PRESS	R^2	RMSD	$k_{1,opt}$
	0.02400	1	0.00032	0.17646	0.95446	0.05423	0.02669
	0.02470	1	0.00036	0.17222	0.95523	0.05358	
	0.02540	1	0.00040	0.16887	0.95574	0.05305	
	0.02610	1	0.00044	0.16636	0.95603	0.05266	
	0.02680	1	0.00048	0.16464	0.95608	0.05238	
	0.02750	1	0.00052	0.16368	0.95593	0.05223	
	0.02820	1	0.00056	0.16341	0.95556	0.05219	
	0.02890	1	0.00059	0.16381	0.95499	0.05225	
	0.02960	1	0.00063	0.16482	0.95423	0.05241	

Appendix 3 The first order rate constants for selective PNPP hydrolysis to validate the results obtained using GRAMS32 software package. The results of GRAMS32 are comparable to one of the Unscrambler software package.

			k (min^{-1})	
$[M]_0$	$[L]_0$	$[M]_0/[T]_0$	GRAMS32	UNSCRAMBLER
0.0200	0.0200	0.5000	9.8935E-03	9.8571E-03
0.0240	0.0160	0.6000	8.3251E-03	8.5337E-03
0.0267	0.0133	0.6675	1.3691E-02	1.3704E-02
0.0286	0.0144	0.715	1.6158E-02	1.6670E-02
0.0300	0.0100	0.7500	8.6825E-03	9.1971E-03
0.0267	0.0133	0.6675	1.5839E-02	1.5965E-02

REFERENCES

1 F. Tafesse and N. C. Deppa, *Ecotoxicol. Environ. Saf.*, 2004, 260-266.

2 V. H. Freed, C. T. Chiou and D. W. Schmedding, *J. Agric. Food Chem.*, 1979, 27(4), 706-708.

3 *Organophosphate insecticides Chapter 4*, Oregon State University, http://npic.orst.edu/RMPP/rmpp_ch4.pdf, 15 November 2006.

4 A. A. Wang, A. Mulchandani and W. Chen, *Appl. Environ. Microbiol.*, 2002, 68(4), 1684-1689.

5 L. Gharahbaghian and T. Bey, *International Journal of disaster medicine*, 2003, 2, 103-108.

6 A. D. F Toy and E. N. Walsh, *Phosphorus Chemistry in Everyday Living*, American Chemical Society, 1987.

7 E. J. Griffith, A. Beeton, J. M. Spencer and D. T. Mitchell, *Environmental Phosphorus Handbook*, John Wiley & Sons, Inc., 1973.

8 Y. Mndubu, MSc Dissertation: *Comparative study for iron mediated hydrolysis of 4-nitrophenyl phosphate in cationic and anionic microemulsion media.*, University of South Africa, 2005.

9 N. C. Deepa, *MSc Dissertation: Metal ion containing microemulsions for the hydrolysis of 4-nitrophenyl phosphate: a model for decontamination of chemical warfare like organophosphate*, Chemistry Department, University of Transkei, Private Bag X1, UNITRA, 2002, 5100.

10 D. Lee, S. Lee, G. H. Seong, J. Choo, E. K. Lee, D. G. Gweon and S. Lee, *Appl. Spectrosc.*, 2006, 60(4), 373-377.

11 P. K. Grzyska, P. G. Czyryca, J. Purcell and A. C. Hengge, *J. Am. Chem. Soc.*, 2003, 125, 13106-13111.

12 O. I. Guliy, O. V. Ignatov, O. E. Makarov and V. V. Ignatov, *Biosens. Bioelectron.*, 2003, 18, 1005-1013.

13 G. H. Rawji, M. Yamada, N. P. Sadler, R. M. Milburn, *Inorg. Chim. Acta.*, 2000, 303(2), 168-174.

14 K. Sorensen-Stowell and A. C. Hengge, *J. Org. Chem.*, 2005, 70, 4805-4809.

15 R. L. Fanshawe, A. G. Blackman and C. R. Clark, *Inorg. Chim. Acta.*, 2003, 342, 114-124.

16 D. R. Jones, L. F. Lindoy and A. M. Sargeson, *J. Am. Chem. Soc.*, 1983, 105, 7327-7336.

17 P. W. A. Hubner and R. M. Milburn, *Inorg. Chem.*, 1980, 19, 1267-1272.

18 F. Tafesse, *Int. J. Mol. Sci.*, 2003, 4, 362-370.

19 J. Rawlings, W. W. Cleland and A. C. Hengge, *J. Inorg. Biochem.*, 2003, 93, 61-65.

20 P. K. Grzyska, P. G. Czyryca, J. Golightly, K. Small, P. Larsen, R. H. Hoff and A. C. Hengge, *J. Org. Chem.*, 2002, 67, 1214-1220.

21 S. G. Srivatsan and S. Verma, *Chem. Commun.*, 2000, 515-516.

22 F. Tafesse, *Inorg. Chim. Acta*, 1998, 269, 287-291.

23 F. Tafesse, *Analyst*, 1997, 122, 293-295.

24 J. Rawlings, A. C. Hengge and W. W. Cleland, *J. Am. Chem. Soc.*, 1997, 119, 542-549.

25 A. C. Hengge, W. A. Edens and H. Elsing, *J. Am. Chem. Soc.*, 1994, 116, 5045-5049.

26 I. R. Jonasson, S. F. Lincoln and D. R. Stranks, *Austral. J. Chem.*, 1970, 23, 2267.

27 H. F Bauer and W. C. Drinkard, *J. Am. Chem. Soc.*, 82, 1960, 5031-5032.

28 S. Armenta, G. Quintas, S. Garrigues and M. de la Guardia, *Trends Anal. Chem.*, 2005, 24(8), 772-780.

29 S. G. Skoulika, C. A. Georgiou and M. G Polissiou, *Appl. Spectrosc.*, 1999, 53(11), 1470-1474.

30 S. G. Skoulika and C. A. Georgiou, *Appl. Spectrosc.*, 2000, 54(5), 747-752.

31 N. Taranenko, J. P. Alarie, D. L. Stokes and T. Vo-Dinh, *J. Raman Spectrosc.*, 1996, 27, 379-384.

32 P. A. Tanner and K. H. Leung, *Appl. Spectrosc.*, 1996, 50(5), 565-571.

33 D. Aslanian, P. Grof, F. Renault and P. Masson, *Biochim. Biophys. Acta*, 1995, 1249, 37-44.

34 S. Farquharson, A. Gift, P Maksymiuk and F. Inscore, *Appl. Spectrosc.*, 2005, 59(5), 654-660.

35 J. G. Dawber, D. R. Brown, R. A. Reed, *J. Chem. Educ.*, 1966, 43(1), 34-35.

36 A. Pintar, J. Batista, J. Levec, *Analyst.*, 2000, 127, 1535-1540.

37 D. B. Chase and J. F. Rabolt, *Fourier Transform Raman Spectroscopy from Concept to Experiment*, Academic Press, INC. A division of Harcourt Brace & Company, 525 B Street, Suite 1900, San Diego, California 92101-4495, 1994, pp1-48.

38 Manu Chopra, PHD Thesis: *Raman Spectroscopic Studies of (A) the Co-C bond in Vitamin B12 and Model Compounds, (B) Inorganic Matrices-Encapsulated Metallocomplexes, and (B) Molecular Hydrogen Compounds*, Georgia Institute of Technology, February

2005, UMI Dissertation Services, A Bell and Howell Company, 300 N, Zeeb Road, Ann Arbor, Michigan 48106, pp1-10.

39 P. Hendra, C. Jones and G. Warnes, *Fourier Transform Raman Spectroscopy, Instrumentation and chemical applications*, Ellis Horwood Limited, Market Cross House, Cooper Street, Chichester, West Sussex, PO19 1EB, England. A division of Simon & Schuster International Group, 1991, 11-48.

40 J. G. Grasselli and B. J. Bulkin, *Anal. Raman Spectrosc.*, John Wiley & Sons, Inc., 1991.

41 D. J. Gardiner and P. R. Graves, *Pract. Raman Spectrosc.*, Springer-Verlag Berlin Heidelberg, 1989, 1-12.

42 H. Baranska, A. Labudzinska and J. Terpinski, *Laser Raman Spectroscopy, Analytical Applications*, PWN-Polish Scientific Publishers, Warsaw, 1987, pp9-31.

43 K. Nakamoto, *Infrared and Raman Spectra of Inorganic and Coordination Compounds Third Edition*, John Wiley & Sons, Inc., 1978, pp3-13.

44 H. A. Szymanski (editor), *Raman Spectroscopy, Theory and Practice*, Plenum Press, 1967, A division of Plenum Publishing Corporation, 227 West 17 street, New York, N.Y. 10011, pp1-4.

45 M. B. Denton, R. P. Sperline, J. H. Giles, D. A. Gilmore, C. J. S. Pommier and R. T. Downs, *Aust. J. Chem.*, 2003, 56, 117-131.

46 S. Fendel and B. Schrader, *Fresenius J. Anal. Chem.*, 1998, 360, 609-613.

47 H. Knozinger and G. Mestl, *Top. Catal.*, 1999, 8, 45-55.

48 W. W. Scheuermann, PhD Thesis: *Raman Spectroscopic Studies of Solids and Liquids By Means of He-Ne Laser Excitation*, December 1970.

49 O. Svensson, M. Josefson and F.W. Langkilde, *Eur. J. Pharm.*, 2000, 11, 141-155.

50 P. Geladi and K. Esbensen, *J. Chemometrics.*, 1990, 3, 337-354.

51 K. Esbensen and P. Geladi, *J. Chemometrics.*, 1990, 4, 389-412.

52 K. H. Esbensen, *Multivariate Data Analysis in Practice 5th edition*, CAMO Press AS, 2002.

53 R. G. Brereton, *Chemometrics Data Analysis for the Laboratory and Chemical Plant*, John Wiley and Sons Ltd, The Atrium, South Gate, Chichester, West Sussex PO 19 8SQ, England, 2003.

54 S. Wold and M. Sjostrom, *Chemom. Intell. Lab. Syst.*, 1998, 44, 3-14.

55 M.P. Fuller, G. L. Ritter and C. S. Draper, *Appl. Spectrosc.*, 1988, 42 (2), 217-227.

56 G. Cruciani, M. Baroni, S. Clementi, G. Costantino, D. Riganelli and B. Skagerberg, *J. Chemometrics.*, 1992, 6, 335-346.

57 A. Lorber and B. R. Kowalski, *Appl. Spectrosc.*, 1990, 44 (9), 1464-1469.

58 E. V. Thomas and D. M. Haaland, *Anal. Chem.*, 1990, 62, 1091-1099.

59 D. M. Haaland, *Anal. Chem.*, 1988, 60, 1208-1217.

60 D. M. Haaland and E. V. Thomas, *Anal. Chem.*, 1988, 60, 1202-1208.

61 D. M. Haaland and E. V. Thomas, *Anal. Chem.*, 1988, 60, 1193-1202.

62 P. Geladi and B. Kowalaski, *Anal. Chim. Acta.*, 1986, 185, 1-7.

63 S. Wold, *Technometrics.*, 1978, 20 (4), 397-405.

64 R. D. Snee, *Technometrics.*, 1977, 19 (4), 415-428.

65 A. Savitzky and M. J. E. Golay, *Anal. Chem.*, 1964, 36 (8), 1627-1639.

66 (a) GRAMS32 Spectroscopic Software, Galactic Industries Corporation, 395 Main Street, Salem, NH 03079-2464 USA.
(b) GRAMS32 PLS-IQ Applications Handbook and Tutorial, Galactic Industries Corporation, Salem, NH 03079-2464 USA.

67 H. Haario and V. M. Taavitsainen, *Chemom. Intell. Lab. Syst.*, 1998, 44, 77-98.

68 V. M. Taavitsainen and H. Haario, *J. Chemometrics.*, 2001, 15, 215-239.

69 S. W. Pennycuick, *J. Am. Chem. Soc.*, 1924, 125, 2049-63.

70 W. W. Floyd, *J. Physical Chem.*, 1931, 35, 2968-84.

71 S. W. Pennycuick, *J. Am. Chem. Soc.*, 1926, 48, 6-19.

72 L. P. Hammett and M. A. Paul, *J. Am. Chem. Soc.*, 1934, 56, 830-2.

73 V. K. Krieble, *J. Am. Chem. Soc.*, 1935, 57, 19-22.

74 J. M. Sturtevant, *J. Am. Chem. Soc.*, 1937, 59, 1528-37.

75 I. W. Sizer, *J. Gen. Physiology.*, 1938, 21, 695-706.

76 J. N. Pearce and M. E. Thomas, *J. Physical Chem.*, 1938, 42, 455-67.

77 P. M. Leininger and M. Kilpatrick, *J. Am. Chem. Soc.*, 1938, 60, 2891-9.

78 L. J. Heidt and C. B. Purves, *J. Am. Chem. Soc.*, 1940, 10, 297-302.

79 C. J. Plank and H. Hunt, *J. Physical Chem.*, 1941, 45, 1403-15.

80 V. Kollonitsch, *Sucrose Chemicals, A Critical View of a Quarter-Century of Research by the Sugar Research Foundation*, The International Sugar Reseach Foundation, Inc., 1970, 11-13 and 136-137.

81 D. P. Shoemaker, C. W. Garland, J. I. Steinfeld and J. W. Nibler, *Experiments in Physical Chemistry Fourth Edition*, McGraw-Hill, Inc., 1981, 271-280.

82 F. A. Bettelheim, *Experimental Physical Chemistry.*, W. B. Saunders Company, 1971, 269-77.

83 J. W. Moore and R. G. Pearson, *Kinetics and Mechanism third Edition.*, 16-9.

84 P. D. Vasko, J. Blackwell and J. L. Koenig, *Carbohyd. Res.*, 1971, 19, 297-310.

85 P. D. Vasko, J. Blackwell and J. L. Koenig, *Carbohyd. Res.*, 1972, 23, 407-16.

86 J. J. Cael, J. L. Koenig and J. Blackwell, *Carbohyd. Res.*, 1974, 32, 79-91.

87 L. D. Barron, A. R. Gargaro and Z. Q. Wen, *Carbohyd. Res.*, 1991, 39-49.

88 S. Soderholm, Y. H. Roos, N. Meinander and M. Hotokka, *J. Raman Spectrosc.*, 1999, 30, 1009-18.

89 P. H. Arboleda and G. R. Loppnow, *Anal. Chem.*, 2000, 72, 2093-98.

90 A. A. Kaminskii, *Crystallography Reports.*, 2003, 48(2), 295-9.

91 M. A. Arnold, G. W. Small, D. Xiang, J. Qui and D. W. Murhammer, *Anal. Chem.*, 2004, 76, 2583-90.

92 T. A. Ring, *Comparison of Raman and ATR-FTIR Spectroscopy of Aqueous Sugar Solutions.*, http://www.che.utah.edu/~ring/Instrumental%20Analysis%20CHE5503/Sample%20Memo%20Report.doc, 21 December 2006.

93 M. Mathlouthi, C. Luu, A. M. Meffroy-Biget and D. V. Luu, *Carbohyd. Res.*, 1980, 81, 213-23.

94 A. N. Batsoulis, N. G. Siatis, A. C. Kimbaris, E. K. Alissandrakis, C. S. Pappas, P. A. Tarantilis, P. C. Harizanis and M. G. Polissiou, *J. Agric. Food Chem.*, 2005, 53, 207-10.

95 M. Mathlouthi, *Carbohyd. Res.*, 1980, 81, 213-23.

96 R. Goodacre, B. S. Radovic and E. Anklam, *Appl. Spectrosc.*, 521-27.

97 *Glycosidic bond – Wikipedia, the free encyclopedia.*, http://en.wikipedia.org/wiki/Glycosidic_bond, 03 January 2007.

98 M. Sekkal, V. Dincq, P. Legrand and J. P. Huvenne, *J. Mol. Struct.*, 1995, 349, 349-52.

99 K. Schenzel and S. Fischer, *Cellul.*, 2001, 8, 49-57.

100 E. C. Corbett, V. Zichy, J. Goral and C. Passingham, *Spectrochim. Acta*, 1991, 47A (9/10), 1399-1411.

101 M. M. Paradkar and J. Irudayaraj, *Food Chem.*, 2001, 76, 231-239.

102 B. Anderson, R. M. Milburn, J. M. Harrowfield, G. B. Robertson and A. M. Sargeson, *J. Am. Chem. Soc.*, 1977, 99(8), 2652-2661.

103 I. Bernal, J. Myrczek and J. Cetrullo, *J. Coord. Chem.*, 1993, 29, 319-336.

104 R. J. Geue and M. R. Snow, *J. Chem. Soc.*, 1971, 2981-2987.

105 S. P. Roe, J. O. Hill and R. J. Magee, *Monatsh. Chem.*, 1991, 122, 467-478.

106 M. Elyoubi, A. Ouasri, H. Jeghnou, A. R. Rhandour, M. C. Dhamelincourt, P. Dhamelincourt and A. Mazzah, *J. Raman Spectrosc.*, 2004, 25, 1056-1062.

107 S. S. Massoud and R. M. Milburn, *Inorg. Chim. Acta.*, 1988, 146, 3-4.

108 R. P. Bontchev, M. N. Iliev, L. M. Dezaneti and A. J. Jacobson, *Solid State Scie.*, 2001, 3, 133-142.

109 H. Abderrazak, M. Dachraoi, M. J. A. Canada and B. Lendl, *Appl. Spectrosc.*, 2000, 54 (11), 1610-1616.

110 A. H. Mazzah, P. Dhamelincourt, A. Mazzah and M. Lazraq, *J. Raman Spectrosc.*, 1998, 29, 1047-1053.

111 G. A. Carriedo, F. J. G. Alonso, P. A. Gonzalez and J. R. Menendez, *J. Raman Spectrosc.*, 1998, 29, 327-330.

112 H. Cheng, I. Nikolic-Hughes, J. H. Wang, H. Deng, P. J. O'Brien, L. Wu, Z. Y. Zhang, D. Herschlag and R. Callender, J. Am. Chem. Soc., 2002, 124, 11295-11306